

DEPENDENCE OF GALAXY STRUCTURE ON REST-FRAME WAVELENGTH AND GALAXY TYPE*

VIOLET A. TAYLOR-MAGER^{1,2}, CHRISTOPHER J. CONSELICE⁴, ROGIER A. WINDHORST³, AND ROLF A. JANSEN³

Draft version October 15, 2018

ABSTRACT

We present a quantitative analysis of the morphologies for 199 nearby galaxies as parameterized with measurements of the concentration, asymmetry, and clumpiness (CAS) parameters at wavelengths from 0.15-0.85 μ m. We find that these CAS parameters depend on both galaxy type and the wavelength of observation. As such, we use them to obtain a quantitative measure of the "morphological k-correction", i.e., the change in appearance of a galaxy with rest-frame wavelength. Whereas early-type galaxies (E-S0) appear about the same at all wavelengths longward of the Balmer break, there is a mild but significantly-determined wavelength-dependence of the CAS parameters for galaxies types later than S0, which generally become less concentrated, and more asymmetric and clumpy toward shorter wavelengths. Also, as a merger progresses from pre-merger via major-merger to merger-remnant stages, it evolves through the CAS parameter space, becoming first less concentrated and more asymmetric and clumpy, and then returning towards the "locus" of normal galaxies. The final merger products are, on average, much more concentrated than normal spiral galaxies.

Subject headings: galaxies: evolution – galaxies: fundamental parameters – galaxies: structure

1. INTRODUCTION

Deep, high-resolution imaging with telescopes such as the Hubble Space Telescope (*HST*) has revealed that the majority of high redshift galaxies are morphologically different from the majority of galaxies nearby. They appear to have morphologies similar to the relatively rare, low redshift irregular and peculiar galaxies (e.g., Driver et al. 1995, 1998; Glazebrook et al. 1995; Abraham et al. 1996; Odewahn et al. 1996; Ellis 1997; Im et al. 1999; van Dokkum et al. 1999; van den Bergh et al. 2000; Conselice et al. 2005; Papovich et al. 2005). The greater percentage of merging galaxies at high redshift suggests that there was an evolution in the number of merging and interacting galaxies throughout the history of the Universe, which supports models of hierarchical galaxy formation (e.g., White 1979; White & Frenk 1991; Cole et al. 1994; Kauffmann et al. 1997; Roukema et al. 1997; Baugh et al. 1998; Nagashima et al. 2001, 2002). To reveal how galaxies assemble and evolve over time, it is therefore essential to conduct detailed comparisons of galaxies as a function of redshift. To carry out these comparisons it is critical to have a representative baseline at $z \sim 0$. We present in this paper a sample of 199 nearby galaxies, observed from the ultraviolet to the optical red, which can be used as an effective comparison to higher redshift sources.

Morphology has also arisen in recent years as a ma-

ajor method for findings major mergers between galaxies and understanding their role in galaxy formation (Conselice 2006). Mergers are predicted to be the dominate factor in galaxy formation within the Cold Dark Matter model (e.g., Cole et al. 2000), and testing this concept in detail is of major importance. Extensive work has gone into improving on the traditional Hubble sequence, which does not distinguish between the large variety of galaxies that fall into the catch-all irregular class (e.g. irregular, peculiar and merging galaxies). It is of particular importance, especially at high redshift, to find a method that quantifies the morphologies of both normal galaxies and the dominant population of irregular/peculiar galaxies. Hubble typing is also a somewhat subjective method of classification that requires visual inspection of each individual galaxy. With the advent of large deep sky surveys that produce images of hundreds to thousands of galaxies at a time, it is essential to develop an automated method of objectively classifying galaxies, using a system that describes something about the physical properties that shape their light distributions, independent of rest-frame wavelength.

One of the parameters developed for use in automated galaxy classification is the concentration index (C) (Abraham et al. 1994, 1996). This parameter measures how centrally concentrated the light distribution is within a galaxy, which is a tracer of the disk-to-bulge ratio. Abraham et al. (1994, 1996) show that classifications through this parameter are less dependent on high spatial resolution than on Hubble type, and thus are more robust at high redshift and in poor ground-based seeing conditions. Schade et al. (1995), Abraham et al. (1996) and Conselice (1997) introduced very basic methods for measuring the rotational asymmetry index (A) to describe the degree of peculiarity and asymmetry in the light distribution of nearby galaxies and galaxies imaged with HST at redshifts of $z \sim 0.5 - 1.2$. The asymmetry index was later vastly improved through the use of standardized radii and centering techniques (Conselice et al. 2000). The asymmetry parameter is particularly

*BASED ON OBSERVATIONS MADE WITH THE NASA/ESA HUBBLE SPACE TELESCOPE, OBTAINED AT THE SPACE TELESCOPE SCIENCE INSTITUTE, WHICH IS OPERATED BY THE ASSOCIATION OF UNIVERSITIES FOR RESEARCH IN ASTRONOMY, INC., UNDER NASA CONTRACT NAS 5-26555. THESE OBSERVATIONS ARE ASSOCIATED WITH HST PROGRAMS #8645, AND 9124.

¹ Department of Physics and Astronomy, Arizona State University, Tempe, AZ 85287-1504

² Carnegie Observatories, 813 Santa Barbara St., Pasadena, CA 91101

³ School of Earth and Space Exploration, Arizona State University, Tempe, AZ 85287-1404

⁴ School of Physics and Astronomy, University of Nottingham, University Park, England NG7 2RD, UK

useful for identifying merging and strongly interacting galaxies, which tend to have very high asymmetries. Another parameter, introduced by Isserstedt & Schindler (1986), quantifies the ratio of smoothly distributed light to the clumped light distribution. This clumpiness index (S) compares the amount of light in star-forming clusters and associations to the light in a more diffuse older disk population, which correlates with hydrogen recombination lines ($H\alpha$) (Takamiya 1999), and gives an indication of the recent star-formation activity within the galaxy (Conselice 2003).

Other authors proposed improved methods of measuring these concentration, asymmetry, and clumpiness (CAS) parameters, making them less sensitive to the choice of galaxy center, surface-brightness cut-offs, signal-to-noise (S/N) ratio, and resolution effects (e.g. Bershadsky et al. 2000; Conselice et al. 2000; Conselice 2003; Lotz et al. 2004). The CAS parameters were found to correlate with each other, as well as other fundamental parameters such as galaxy color, luminosity, size, surface-brightness, and star formation rate (Isserstedt & Schindler 1986; Abraham et al. 1996; Takamiya 1999; Bershadsky et al. 2000; Corbin et al. 2001). Galaxy types are separated-out within parameter spaces involving color, surface-brightness, and various combinations of the CAS parameters, providing a method of galaxy classification that is relatively robust over a large range of redshifts (Bershadsky et al. 2000; Conselice et al. 2000, Conselice et al. 2003; Conselice 2003).

Galaxies, however, can look substantially different at shorter wavelengths than at longer ones (e.g., Bohlin et al. 1991; Hill et al. 1992; Kuchinski et al. 2000, 2001; Marcum et al. 2001; Windhorst et al. 2002). Hence, if the morphological k -correction is significant, CAS measurements for low redshift galaxies in rest-frame optical light and high redshift galaxies in rest-frame ultraviolet light may not be directly comparable. For example, Schade et al. (1995) found that their galaxies ($z \sim 0.5 - 1.2$) looked more irregular in their B images (rest-frame UV) than at longer wavelengths, which will all have an effect on quantitative galaxy parameters. Jansen (2000) noted a similar systematic shift from U to R for galaxies in the Nearby Field Galaxy Survey. We also observe this effect when comparing HST/WFPC2 UV and near-infrared (IR) images available for a subset of the galaxies presented in Windhorst et al. (2002). In the present paper, we quantitatively analyze how the CAS parameters vary as a function of rest-frame wavelength and morphological type for a sample of 199 nearby galaxies observed in a combination of nine pass-bands ranging from the far-UV to the near-IR. We will apply these results to the high redshift Universe in a future paper (Conselice, et al. 2007, in preparation).

2. OBSERVATIONS

As described in detail in Taylor et al. (2005), we have selected for study a sample of 199 nearby galaxies that consists mostly of late-type spiral, irregular, and peculiar/merging galaxies. These late-types are among the galaxies at $z \sim 0$ that most resemble the majority of high redshift galaxies, and are less studied and less well-understood than nearby earlier-type galaxies. Also, Jansen (2000) found that most of the wavelength dependence of the asymmetry is due to galaxies of type Sbc

and later (de Vaucouleurs type, $T \gtrsim 4$). Thus, most of the difference in asymmetries between the U and R -band occurs for later morphological Hubble types. As such, late-type galaxies are more suited for this analysis than early-type galaxies. The selected morphological distribution for our sample is shown in Figure 1. For a discussion of the effects of this deliberate type pre-selection, see Windhorst et al. (2002).

Of the 199 galaxies in our sample, 143 were observed with the Vatican Advanced Technology Telescope (VATT) in $UBVR$ ($\lambda_c = 3597, 4359, 5395,$ and 6338\AA , respectively). A total of 90 galaxies were observed with HST WFPC2 in the UV (F300W, $\lambda_c = 2930\text{\AA}$), 34 of which also have VATT data. Of these 90 galaxies observed with HST, 37 were observed in our Cycle 9 GO program #8645 (Windhorst et al. 2002; Taylor et al. 2005), and 53 were observed in our Cycle 10 SNAP-shot program #9124 (P.I.: R. Windhorst; Jansen et al. 2007, in preparation). During these programs, a subset of 11 galaxies were also imaged with a shorter wavelength UV filter (F255W, $\lambda_c = 2550\text{\AA}$), and 60 were observed in the red (F814W, $\lambda_c = 8230\text{\AA}$). Taylor et al. (2004, 2005) give a more detailed description of these observations. At the time the present analysis was completed, 13 of the galaxies in our sample had deep ($t_{exp} \gtrsim 670$ s) GALEX mid-UV (NUV, $\lambda_c = 2275\text{\AA}$) and far-UV (FUV, $\lambda_c = 1550\text{\AA}$) imaging available. A 14th galaxy, NGC0569, was observed only in the GALEX NUV filter. Of these, 4 were observed with our GALEX Cycle 1 SNAP program #036, and 10 were obtained from the archived Nearby Galaxies Survey (NGS), Medium Imaging Survey (MIS), and Deep Imaging Survey (DIS) (Martin et al. 2005; Heckman et al. 2005). Seven of the 14 galaxies observed with GALEX also have VATT data, and 10 also have HST data. Three of these galaxies have data from all of these telescopes (VATT, HST, and GALEX).

In Table 1 we identify the galaxies in our sample, and list their relevant global properties. The first 25 galaxies are listed here, with the full table available in the electronic edition. Column (1) lists the galaxy identification numbers as used throughout this paper, while column (2) gives the common catalog names, and columns (3) and (4) contain the equatorial coordinates (J2000.0). Column (6) and (7) lists the total ($B - V$) color and their errors (respectively), as measured from the galaxies for which we have B and V images, or from the RC3 (de Vaucouleurs et al. 1991) otherwise. All recessional velocities with respect to the Galactic Standard of Rest (V_{GSR} ; column 8) are from the RC3. In column (9), we identified the edge-on spiral galaxies in our sample. The numeric types adopted throughout the present paper are listed in column (5), and were assigned as described in section 4.1. Figure 1 shows the distribution of morphological types within our sample. Note the deliberate emphasis on late-type galaxies for the purposes of high redshift comparison.

3. DATA REDUCTION

The $UBVR$ CCD images obtained at the VATT were reduced and calibrated as described in Taylor et al. (2004, 2005). For the data analysis in these previous papers, all of the non-target objects in the images were replaced with a constant local sky-level. This was suitable for computing radial profiles of surface-brightness

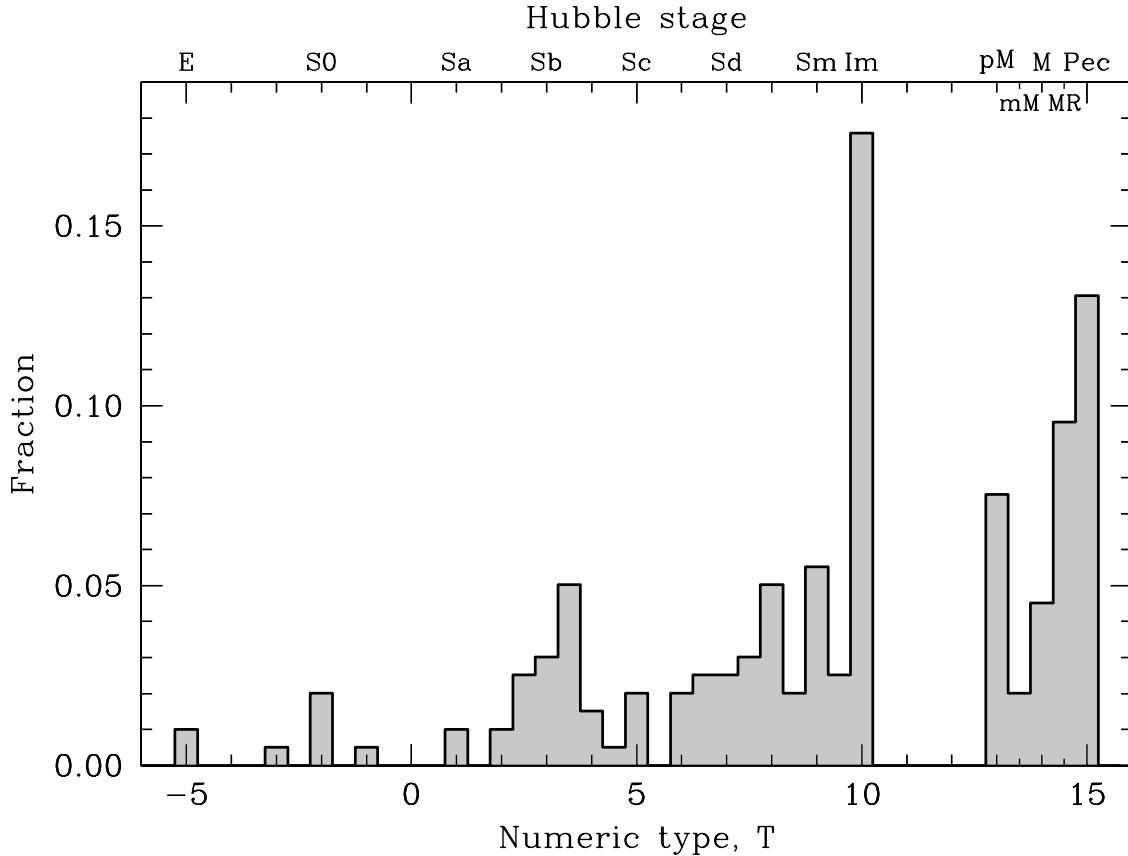


FIG. 1.— Distribution of types within the present sample of nearby galaxies. Since the vast majority of galaxies observed at high redshift display morphologies resembling those of nearby late-type spiral, irregular, and peculiar/merging galaxies, our sample is intentionally heavily weighted toward such galaxy types. The subdivision of types later than 11 is discussed in the text, and in Hibbard et al. (2001).

and color, which are not sensitive to structure on small scales within a galaxy. However, the deviations from the true underlying galaxy light distribution at the locations of non-target objects, as replaced with the local sky-level, are larger than is acceptable for CAS measurements, which are particularly sensitive to high spatial frequency structure within the galaxy. Therefore, in these cases we applied a more sophisticated means of removing the non-target objects, interpolating from adjacent pixels with valid data over these masked pixels along both the vertical and horizontal directions (implemented by R. Jansen as task *IMCLEAN*⁵ within *IRAF*⁶). This routine preserves the surrounding sky properties as much as possible inside the interpolated region.

We obtained stacked images for most of our HST Cycle 9 galaxies as type B associations from the Space Telescope Science Institute (STSCI) data archive.⁷ Seven of the Cycle 9 images do not have associations available for at least one of the filters. These individual images were thus combined and cosmic-ray rejected using an IDL routine developed by Cohen et al. (2003). The HST Cycle 10 images were combined using an *IRAF* task devel-

oped by R. Jansen, that rejects bad pixels based on the noise characteristics of the images (Jansen et al. 2007, in preparation). For each galaxy, the stacked images for the individual WFPC2 CCD's were then mosaiced using the *WMOSAIC* task within the *STSDAS* package in *IRAF*. Non-target objects were interpolated-over with *IMCLEAN*.

We retrieved pipeline processed images of each of the sample galaxies observed by GALEX through the STSCI data archive. Since GALEX has a field-of-view of 1.2° , and most of our galaxies are only around $1'$ in size, we cut 512×512 pixel GALEX stamps centered on our target galaxy for use in the data analysis. This corresponds to an image size of about $12'$, which is sufficient for viewing the entire galaxy and measuring the sky from surrounding regions that are far enough away from the galaxy that they are uncontaminated by its light. Non-target objects were interpolated-over with *IMCLEAN*, as before.

4. DATA ANALYSIS

4.1. Visual Classifications

We assigned visual types to these galaxies using the average of three experienced classifiers to classify the galaxies observed with the VATT (Taylor et al. 2005), and the average of two experienced classifiers (V. Taylor, and C. Conselice) for the galaxies observed with HST. For each of the normal galaxies in our sample, we assigned morphological types on the numeric 16-step de Vaucouleurs system, which ranges from $T = -5$ (Elliptical) through

⁵ <http://www.public.asu.edu/~rjansen/>

⁶ *IRAF* is distributed by the National Optical Astronomy Observatories, which are operated by the Association of Universities for Research in Astronomy, Inc., under cooperative agreement with the National Science Foundation.

⁷ <http://archive.stsci.edu/hst/wfpc2/index.html>

TABLE 1
OBSERVED GALAXY LIST.

ID# (1)	Galaxy (2)	RA (3)	DEC (4)	Type (5)	B-V (6)	σ_{B-V} (7)	V_{GSR} (8)	comment (9)
001	UGC00006	00:03:09.46	+21:57:37.6	15.0	0.370	0.040	6763	...
002	NGC0014	00:08:46.32	+15:48:56.4	10.0	0.580	0.035	1012	...
003	UGC00156	00:16:46.30	+12:21:13.1	9.3	0.576	0.042	1267	...
004	NGC0178	00:39:08.25	-14:10:20.7	9.5	0.470	0.040	1496	...
005	UGC00404	00:39:19.17	+13:06:40.3	13.0	0.362	0.030	10742	...
006	Mrk960	00:48:35.44	-12:42:59.9	8.0	...	0.024	6447	...
007	UGC00512	00:50:02.59	+07:54:55.3	15.0	-0.004	0.017	5496	...
008	UGC00644	01:03:16.65	+14:02:01.6	13.0	0.662	0.013
009	UGC00685	01:07:22.29	+16:41:04.1	10.0	...	0.010	271	...
010	UGC00749	01:11:30.28	+01:19:10.9	14.5	0.653	0.006	6882	...
011	NGC0428	01:12:55.62	+00:58:52.2	9.0	0.440	0.014	1231	...
012	UGC00849	01:19:23.03	+12:26:57.4	14.5	0.572	0.015	14410	...
013	NGC0569	01:29:07.16	+11:07:53.3	13.0	...	0.013	5862	...
014	UGC01104	01:32:43.47	+18:19:01.4	10.0	0.533	0.018	775	...
015	UGC01133	01:35:00.85	+04:23:11.8	15.0	0.077	0.014	2031	...
016	NGC0625	01:35:05.12	-41:26:08.9	10.0	0.560	0.016	312	...
017	UGC01219	01:44:20.13	+17:28:42.9	3.0	0.709	0.015	4708	...
018	UGC01240	01:46:19.56	+04:15:52.5	15.0	0.401	0.015	1862	...
019	UGC01449	01:58:04.15	+03:05:57.2	14.0	0.487	0.015	5590	...
020	UGC01753	02:16:34.98	+28:12:16.1	8.7	0.559	0.038	3098	...
021	NGC0959	02:32:23.45	+35:29:20.1	7.0	0.588	0.009	715	...
022	NGC1140	02:54:33.43	-10:01:42.4	15.0	0.350	0.008	1479	...
023	NGC1156	02:59:41.41	+25:13:37.5	10.0	0.618	0.009	452	...
024	NGC1311	03:20:06.66	-52:11:12.5	10.0	0.460	0.021	331	...
025	ESO418-G008	03:31:30.58	-30:12:46.6	8.0	0.410	0.012	1146	...

NOTE. — **Columns:** (1) ID number assigned to this galaxy, (2) galaxy name, (3) Right Ascension (J2000), (4) Declination (J2000), (5) classification (de Vaucouleurs numerical types were used for normal galaxies, with the following types assigned to peculiar/merging galaxies (see text for details): 13.0=pre-merger, 13.5=minor merger, 14.0=major merger, 14.5=merger remnant, 15.0=peculiar), (6) total ($B - V$) color (mag), (7) uncertainty on ($B - V$), (8) Galactic standard of rest velocity (km s^{-1}), and (9) special comment for this galaxy. "Edge-on" galaxies appear to be edge-on spiral galaxies. The full table is available only in the electronic edition.

$T = 10$ (irregular). The median difference between classifications by individual classifiers was zero, with 75% of the classifications agreeing to within ± 1 T-type-bin, and all agreeing to within ± 4 bins. For merging and peculiar galaxies, we used the following typing scheme, which was partially adapted from Hibbard et al. (2001). Pre-mergers (pM, $T = 13.0$) are galaxies that are tidally interacting with another nearby galaxy, but they are at a large enough distance from each other that the individual galaxies can be easily distinguished and treated separately. Minor mergers (mM, $T = 13.5$) are two or more galaxies showing signs of merging, in which one of the galaxies is much larger or brighter than the others (estimated to be at least about 4 times larger or brighter). Major mergers (M, $T = 14.0$) are galaxies of apparently similar mass or luminosity that are interacting or merging. Major merger remnants (MR, $T = 14.5$) are objects in the later stages of merging, such that it is difficult to say exactly what has merged, when, or how. Peculiar galaxies (P, $T = 15.0$) are abnormal or unclassifiable galaxies which do not fit on the normal Hubble sequence, but were not obviously involved in a merger. A subset of these may, however, be late-stage merger remnants. Figure 2 shows an example of each of the four major types of merging galaxies.

4.2. CAS Parameter Measurements

We adopt the definitions of the CAS parameters of Conselice et al. (2000) and Conselice (2003), as de-

scribed below, and measured CAS parameters for our galaxy sample using the IRAF task CAS, developed by C. Conselice (Conselice et al. 2000; Conselice 2003).

The concentration index, C , is computed by determining the total sky-subtracted light contained within $1.5 \times$ the Petrosian radius (r_{Pet}) (Petrosian 1976), and finding the logarithmic ratio of the radius within which 80% of this light is contained (r_{80}) to the radius within which 20% of this light is contained (r_{20}) (Conselice et al. 2000). The concentration index is thus given by the formula:

$$C = 5 \times \log(r_{80}/r_{20}) \quad (1)$$

Therefore, galaxies that are highly concentrated in their centers (e.g., ellipticals) will have high values of C , and galaxies that have less-centrally concentrated light distributions (e.g., disk galaxies or low surface-brightness galaxies) will have lower values of C .

The asymmetry index, A , is computed by rotating the galaxy by 180° from its center, and subtracting the light within $1.5 \times r_{Pet}$ in the rotated image (I_{180}) from that in the original image (I_o). The ratio of the residual subtracted flux to the original galaxy flux yields A :

$$A = \min\left(\frac{\sum |I_o - I_{180}|}{\sum |I_o|}\right) - \min\left(\frac{\sum |B_o - B_{180}|}{\sum |I_o|}\right) \quad (2)$$

Noise corrections were applied by subtracting the asymmetry of an empty background region (B), and iterative centering corrections were applied to minimize A , since gross centering errors would artificially increase A .

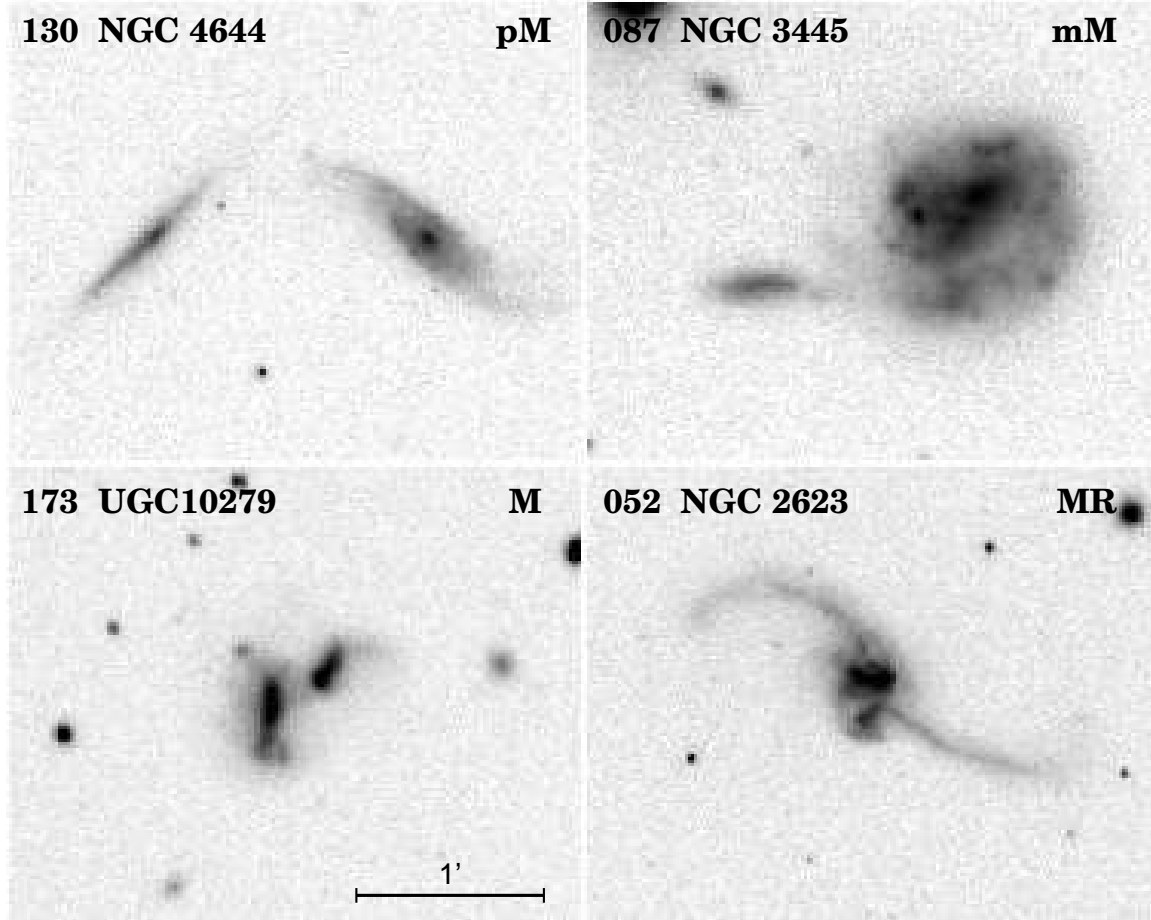


FIG. 2.— Examples of the sub-classifications assigned to the merging galaxies in our sample. Each of the the B-filter VATT images measures $3.0' \times 2.4'$. **Top left:** NGC4644 (the galaxy on the right) is in strong interaction with its neighbor NGC4644B (PGC42725), and is classified as a pre-merger (pM). **Top right:** NGC3445 appears to be accreting a smaller companion, PGC32784, and is classified as a minor merger (mM). **Bottom left:** UGC10279 represents a major merger event (M) between two galaxies of similar mass, Holmberg 734A and B. **Bottom right:** in NGC2623 the properties of the galaxies that merged are no longer exactly discernible, so it is classified as a merger remnant (MR, early stage).

Asymmetries range from $A = 0$ to 2, with $A = 0$ corresponding to a truly symmetric galaxy (e.g., some ellipticals; see Jansen(2000) for an example of a highly symmetric spiral galaxy), and $A = 2$ corresponding to a completely asymmetric galaxy.

The clumpiness index, S , is defined as the ratio of the amount of light in high spatial frequency structures within $1.5 \times r_{Pet}$ to the total amount of light in the galaxy within that radius (Conselice 2003). This was done by subtracting a boxcar-smoothed image from the original image to produce an image that contains only the high-frequency structure. The central pixels within $1/20$ th of the total radius were set to zero to exclude them from the parameter measurements. S is given by the following equation, where $I_{x,y}$ is the intensity of light in a given pixel, $I_{x,y}^s$ is the intensity of that pixel in the image smoothed by $0.3 \times r_{Pet}$, and $B_{x,y}^s$ is an intensity value of a pixel from a smoothed background region:

$$S = 10 \times \left(\frac{\sum_{x,y=1,1}^{N,N} (I_{x,y} - I_{x,y}^s)}{\sum_{x,y=1,1}^{N,N} I_{x,y}} - \frac{\sum_{x,y=1,1}^{N,N} B_{x,y}^s}{\sum_{x,y=1,1}^{N,N} I_{x,y}} \right) \quad (3)$$

A clumpiness of $S = 0$ corresponds to a galaxy that has no high frequency structure, and is therefore completely

smooth (e.g., some ellipticals that are far enough away that they are not resolved into their brightest stars). Galaxies with more high-frequency structure are more patchy in appearance, and will have a higher value of S .

5. RESOLUTION AND SIGNAL-TO-NOISE EFFECTS

The effects of spatial resolution on the CAS parameters are discussed in detail in Conselice (2003) and Conselice et al. (2000). Previous studies have shown that a spatial resolution (R) of ~ 1 kpc is at the limit beyond which poorer resolution will affect the measurements, with asymmetry parameters determined with HST/WFPC2 becoming unreliable for the more distant galaxies in the Hubble Deep Field (Conselice et al. 2000; Lotz et al. 2004). At resolutions better than this limit, Conselice (2003) found that the asymmetry index does not depend strongly on the resolution or seeing of the image, with 70% of the value of A , as measured in the optical, attributable to overall global distortions in the galaxy, and 30% due to localized high-frequency structures, such as star-forming regions. Low S/N ratios within the galaxy can also decrease the reliability of the CAS measurements (Conselice et al. 2000; Lotz et al. 2004). Conselice et al. (2000) found that asymmetries can be computed most

reliably when the integrated S/N ratio $\gtrsim 100$ per object. These S/N and resolution reliability limits, however, are rather conservative, and would result in poor (or no) number statistics in some of our galaxy typebins. Therefore, in this section we will investigate the effects of S/N and spatial resolution in our data, and determine the limits of each that are appropriate for our analysis. We determined the spatial resolution in kpc from the recessional velocities listed in the RC3 (using V_{GSR} when available, or V_{hel} otherwise). Total S/N ratios were measured within 1.5 times the Petrosian radius.

5.1. The Effects of Smoothing the HST data

For the *UBVR* images observed at the VATT, the images of each galaxy were convolved to the worst seeing for that galaxy (typically in the *U*-band), using a Gaussian of the appropriate width within the task **GAUSS** in IRAF. The seeing of each image was determined by finding the average FWHM (full width at half max) of all stars detected with SExtractor (Bertin & Arnouts 1996), as described in detail in Taylor et al. (2004).

In order to consistently compare images of a galaxy with ground-based seeing to those from HST/WFPC2 (FWHM $\sim 0''.14$), it may be necessary to convolve the HST images to the same resolution as the ground-based data. We test this by examining the effect on the CAS parameter measurements after convolving the HST images (as for the VATT) to the $1''.75$ average *U*-band seeing at the VATT. The left three panels in Figure 3 show the difference between the CAS measurements from the convolved and unconvolved HST images in each filter vs. the measurements in the unconvolved images. The right-most panels show the median of these differences for each filter. Horizontal dotted lines indicate when convolution does not affect the CAS parameters. Different symbols in Figure 3 are used for measurements from images where the galaxy had low S/N (large open squares: $S/N < 75$, small open squares: $75 < S/N < 100$), and where the galaxy had low physical resolution (large open triangles: $R > 1.25$ kpc, small open triangles: $1.00 < R < 1.25$ kpc). There is no real trend with low S/N or spatial resolution, although most of the extreme outliers have low S/N or, in exceptional cases, low resolution.

The differences between CAS parameters at the two different resolutions are most pronounced in the F255W images, which had the lowest S/N ratio, and thus the highest uncertainties in these parameters. Convolution of these images resulted in boosting the signal in each resolution element, as well as smoothing over high-frequency structure in the noisy background, which is strongly affected by charge transfer effects (CTE). This results in more reliable CAS values that are not as severely affected by spikes in the sky background, as can be seen by considering the *A* and *S* panels in Figure 3. Vertical dotted lines in these panels represent the limit below which the *A* and *S* values measured in the sky were higher than those measured in the galaxy ($A < 0$, $S < 0$). For these extreme cases, convolving the images increased the signal and decreased the noise, which resulted in increasing most of the negative values of *A* and *S* into the positive regime. CTE-noise effects are also present in the data from the other WFPC2 filters, although it is not as strong of a factor in the longer wavelength pass-bands due to the higher S/N ratio of the galaxies and the more

significant zodiacal sky-brightness filling in the low-level CTE-traps. A combination of smoothing over the noise and the high-frequency structure of the galaxy itself has an effect on the CAS parameters in all filters, to varying extents.

Overall, the concentration index does not change significantly with spatial resolution, especially at longer wavelengths. The median values of the change in *C* after convolving the HST images to the ground-based seeing are 0.228, -0.002 , and -0.028 in F255W, F300W, and F814W, respectively (these values will be given in this filter order for the rest of this paragraph). This is marginally greater than the median uncertainty on the individual unconvolved values of *C* in F255W (0.209), and well within the median uncertainties in F300W and F814W (0.030 for both). The asymmetry index is more affected by convolution, although there is no trend in this effect with increasing *A*. This is likely due to a boost in S/N per resolution element, which improves the reliability of the measurement (Lotz et al. 2004). Convolution of the images to the ground-based seeing changed *A* by a median value of 0.369, 0.083, and -0.021 , respectively. Except for the noisy F255W images, this is roughly within the median uncertainties of 0.181, 0.078, and 0.044, respectively. The clumpiness index, however, was more strongly affected by the resolution change, with intrinsically clumpy galaxies showing a strong trend in all filters toward decreasing clumpiness with decreasing resolution. This is to be expected, as *S* is designed to measure high-frequency structure, and star clusters and associations may be resolved in the unconvolved HST images. Convolution of the images changed the median *S* by 0.840, -0.780 , and -0.215 , respectively. These are relatively significant differences, and much larger than the median uncertainties on *S* of 0.249, 0.256, and 0.135, illustrating that real structure being smoothed over lowers the measured *S* values.

With the above caveats, throughout the remainder of this paper we therefore use the CAS values measured in HST images convolved to match the resolution of our ground-based VATT images, to reduce the effects of background noise and to offer a more systematic comparison. We note that with the exception of F814W, this does not do gross injustice to the high resolution HST images, since the F255W and F300W filters are below the atmospheric cut-off, and therefore are unique data even at lower resolution.

5.2. Determining a S/N and Resolution Reliability limit

Of the 143 galaxies observed with the VATT, 16 have spatial resolutions between 1.00 and 2.20 kpc in the *U*-band image, which is above the reliability limit of 1 kpc quoted in Conselice et al. (2000). Only one galaxy (UGC01133 in the *V*-band) was found to have a S/N ratio below the Conselice et al. (2000) reliability limit of 100. These limits (hereafter referred to as $limit_1$) are conservative, however, so it may be acceptable to use more relaxed limits in the interest of conserving higher number statistics. If we relax the limits by 25% (defined as $limit_2$), we find 9 galaxies with $R > 1.25$ kpc, and no galaxies with $S/N < 75$.

Of the 90 galaxies observed with the HST in F300W (11 of which were also observed in F255W, and 60 in F814W), 6 have $1.00 < R < 1.44$ kpc, and 2 have R

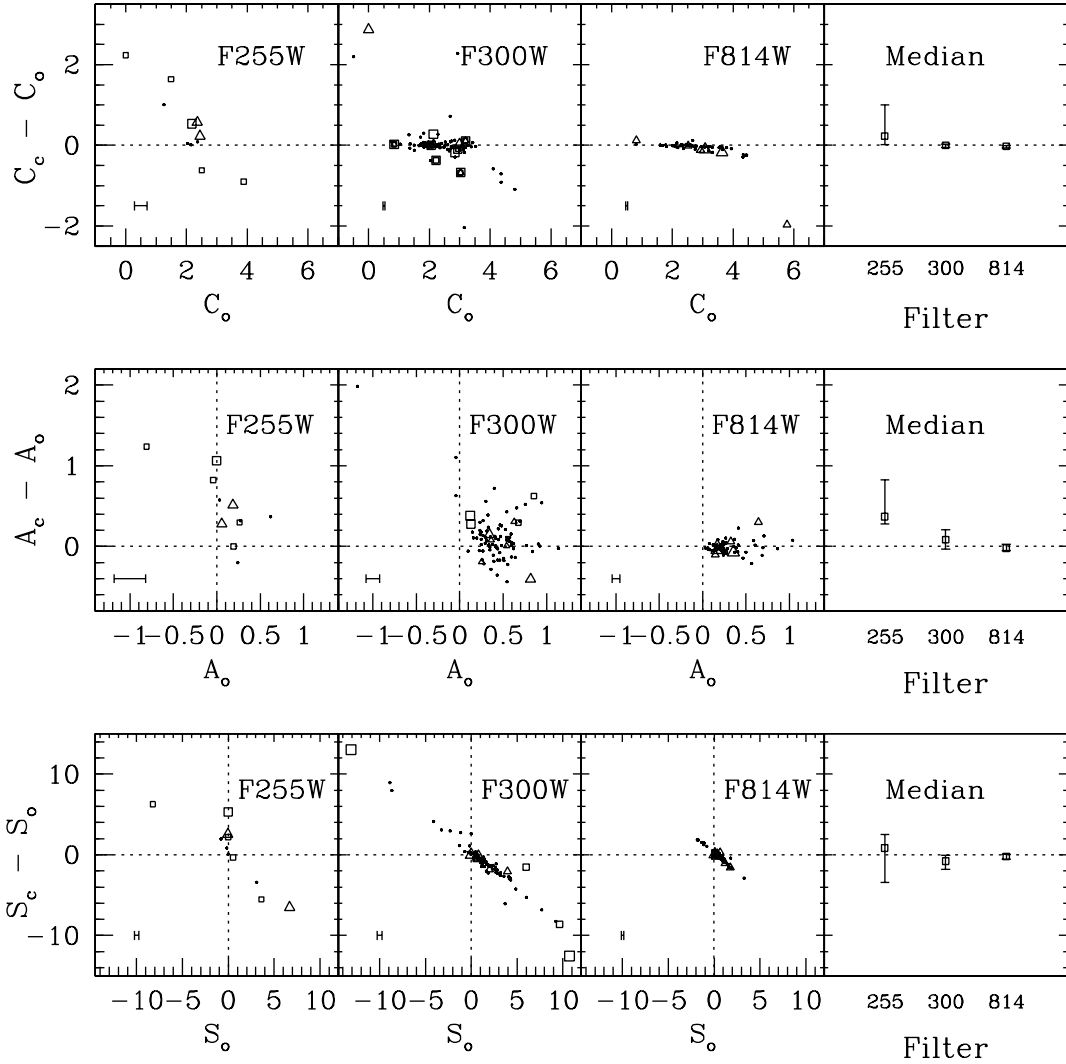


FIG. 3.— The difference between CAS parameters measured from HST images convolved to the average VATT ground-based seeing of $1.75''$ (X_c), and those measured from the original high resolution ($0.14''$ FWHM) HST images (X_o), plotted versus the measurements in the original images. *Open square symbols* represent galaxies with low S/N (*large symbols*: $S/N < 75$, *small*: $75 < S/N < 100$). *Open triangle symbols* represent galaxies with low spatial resolution (R) in the convolved images (*large*: $R > 1.25$ kpc, *small*: 1.00 kpc $< R < 1.25$ kpc). **Left 3 panels:** *TOP*: Change in concentration index, $C_c - C_o$, versus C_o . *MIDDLE*: Change in asymmetry index, $A_c - A_o$, versus A_o . *BOTTOM*: Change in clumpiness index, $S_c - S_o$, versus S_o . Each panel shows data from a different pass-band, as labeled in the panels. The horizontal error bar in the lower left corner of each panel represents the median uncertainties for each parameter in the original images. **Right-most panels:** Median difference in each filter between C_c and C_o (top), A_c and A_o (middle), and S_c and S_o (bottom). Error bars represent the 25% - 75% quartile range. Horizontal dotted lines indicate where the value of the CAS parameter did not change between the convolved and unconvolved images. Vertical dotted lines in the A and S panels represent the cut-off below which the A and S measurements of the sky were larger than those of the galaxy. Most of these outlying values were increased to positive values after convolving the images.

> 1.25 kpc. In F255W, 7 galaxies have $S/N < 100$, and 3 have $S/N < 75$. In F300W, 5 galaxies have $S/N < 100$, and 2 have $S/N < 75$. All galaxies observed in F814W have $S/N > 100$.

The GALEX images have a stellar FWHM of $\sim 5''$, which is $\sim 3\times$ larger than that of the VATT and the convolved HST data. The CAS values, however, should still be reliably determined, as long as the spatial resolutions of the galaxies are within the above reliability limit. Of the 14 galaxies observed with GALEX, 7 have $R > 1.00$ kpc, with resolutions between 1.41 and 2.37 kpc. One

additional galaxy (NGC1396) was barely detected in the FUV.

The main goal of this work is to determine the general trends of the CAS parameters, mainly through the use of the median values for each type-bin and filter. For well-populated bins of type and filter, imposing conservative reliability limits improves the significance of the median values. In several of our sparsely populated bins, however, measurement uncertainties and peculiarities of individual galaxies would dominate. If we can relax the Conselice et al. (2000) limits of $S/N > 100$ and $R < 1.00$

kpc (limit_1) without having a significant effect on the median CAS values, we can then improve the number statistics in our type-bins while still obtaining reasonably high reliability. As such, we have tested the effects of applying limit_1 to our relatively well-sampled VATT and HST F300W and F814W data set against applying a more liberal limit of $S/N > 75$ and $R < 1.25$ kpc (limit_2). Table 2 summarizes the results. The median CAS parameters in each type-bin were calculated for the entire data set ("all"), and separately for those data meeting each of the reliability requirements we are considering (limit_1 and limit_2). Since we find little difference in the results between filters for each telescope, we average the medians over U , B , V , and R for the VATT, and over F300W and F814W for HST. Table 2 lists the difference between these medians calculated with limit_1 and all of the data, and also the difference between the medians calculated with limit_1 and limit_2 . The final column in Table 2 gives the average uncertainty on the difference between the medians for a given parameter observed with the VATT or HST. These uncertainties were calculated by taking the quadratic sum of the median range of CAS values, averaged over the relevant filters, and normalized by the square-root of the average number of galaxies per type-bin. Although in a few individual sparsely populated type-bins the median CAS values are affected at the $\gtrsim 1\sigma$ level, we find that for the vast majority of bins the median values do not change by relaxing our limits on minimum S/N and spatial resolution from limit_1 to limit_2 . This is also the case for the GALEX and F255W data.

Applying limit_1 results in an average change with respect to no limit in the median C, A, and S values, respectively, of 0.051 ± 0.035 , 0.004 ± 0.018 , and -0.002 ± 0.064 . Within the uncertainty on these averages, only the concentration index is affected by the application of limit_1 . Applying limit_2 results in an average change from the values calculated with limit_1 of -0.034 ± 0.035 , 0.002 ± 0.018 , and 0.013 ± 0.064 , in C, A, and S, respectively. All of these are within the uncertainties, although only marginally so for C. Therefore, we find that it is acceptable to apply the somewhat more relaxed reliability limits of limit_2 to our analysis, in order to retain adequate sample sizes. In the subsequent plots, data points that do not satisfy our S/N and resolution criteria (limit_2) will be plotted using smaller symbols, but not used to calculate the presented trends. Applying this limit results in the rejection of 8 of the 13 galaxies in FUV, 7/14 in NUV, 3/11 in F255W, 4/90 in F300W, 9/143 in $UBVR$, and 2/60 in F814W. It is clear that the FUV, NUV, and F255W data are barely adequate for the current studies, and only instruments like WFC3 (to be launched to HST in SM4) can significantly improve on this.

6. RESULTS

6.1. Relating CAS Parameters to Galaxy Color and Type

Tables 3, 4, and 5 list our C, A, and S measurements and errors, respectively, for each galaxy in each pass-band. The first 25 galaxies are listed here, with the full tables available in the electronic edition. Ellipsis indicate that there are no images available for that galaxy in that particular pass-band. Footnotes mark measure-

ments for images in which the galaxy did not meet the S/N or resolution requirements of our adopted limits ($S/N < 75$ or $R > 1.25$ kpc). Figures 4, 5, and 6 show the C, A, and S parameters, respectively, versus the total ($B - V$) color of each galaxy. Values for each pass-band are shown in separate panels within each figure, with different colored symbols used to designate early-type (E-S0), mid-type (Sa-Sc), late-type (Sd-Im), and peculiar/merging galaxies, as indicated by the legend in Figure 4. Smaller symbols represent galaxies that are below the reliability limits adopted in Section 5.2 ($S/N < 75$, or $R > 1.25$ kpc). Representative error bars are shown in each panel with the median uncertainty in the CAS parameters of the individual data points, and the average ($B - V$) uncertainty of 0.04 mag. These figures show a trend of galaxies becoming generally more concentrated, less asymmetric, and less clumpy with redder ($B - V$) color. There is a large spread and overlap of these parameters with galaxy type, so that galaxy classifications made from these plots can only be used as approximate indicators. Early-type galaxies are most clearly separated from the later galaxy types, since they are the reddest, the most concentrated, the least asymmetric, and the least clumpy. Later galaxy types are increasingly bluer, less concentrated, more asymmetric, and more clumpy than earlier galaxy types. This result is in agreement with previous authors (e.g. Takamiya 1999; Bershady et al. 2000; Conselice et al. 2000, 2003; Conselice 2003). There is a much higher spread in S at shorter wavelengths, with a CAS- $(B - V)$ correlation that changes slope with filter, such that blue galaxies tend to be more clumpy at shorter wavelengths than they are at longer wavelengths, although the statistics in the UV are scarce. This logically results from bluer late-type galaxies containing more recent star formation, and therefore having more blue knots from recently formed star clusters and associations that will increase the clumpiness in the bluer filters. The CAS values of peculiar/merging galaxies vary considerably, but their median values are slightly offset from the locus of normal galaxies, with peculiar/merging galaxies being generally bluer (by 0.03 mag), and slightly more concentrated (by ~ 0.2) and asymmetric (by ~ 0.1). These type-dependent offsets and their overlap are discussed in more detail below.

Figures 7, 8, and 9 show the C, A, and S parameters, respectively, of each galaxy as a function of galaxy type. As for Figures 4–6, separate panels show results from different filters. Data-points from galaxies that did not meet the reliability criteria ($S/N < 75$, or $R > 1.25$ kpc) are indicated with small black points. Median values of the CAS parameters in a particular filter within a particular type-bin are indicated with large colored symbols, and the spread of the data points is indicated by the 25–75% quartile range, represented by the vertical error bars. These median C, A, and S values are also listed in Tables 6, 7, and 8, respectively. Data that did not meet the reliability criteria were not included in the medians. Due to low S/N and significant CTE effects (particularly in F255W) causing the clumpiness measured in the sky to be higher than that measured in some galaxies, median values of S were only calculated with data that had $S > -0.2$. In all three plots, the spread in the CAS parameters increases toward later galaxy type. There are few objects in the GALEX FUV

TABLE 2
CHANGE IN MEDIAN CAS PARAMETERS WITH RELIABILITY LIMITS

Parameter (1)	Telescope (2)	Difference (3)	E–S0 (4)	Sa–Sc (5)	Sd–Im (6)	Pm (7)	mM (8)	M (9)	MR (10)	P (11)	σ_{med} (12)
C	VATT	limit ₁ –all	0.120	0.000	0.000	-0.005	0.358	0.183	-0.030	0.053	0.10
C	VATT	limit ₁ –limit ₂	-0.120	-0.015	0.000	0.000	-0.358	0.245	0.035	-0.053	0.10
C	HST	limit ₁ –all	0.000	0.045	-0.040	-0.195	0.000	0.435	-0.105	0.000	0.10
C	HST	limit ₁ –limit ₂	0.000	-0.065	0.020	0.195	0.000	-0.435	0.000	0.000	0.10
A	VATT	limit ₁ –all	-0.008	-0.003	0.000	0.030	0.088	-0.113	0.008	0.003	0.04
A	VATT	limit ₁ –limit ₂	0.008	0.000	0.000	0.000	-0.088	0.115	-0.008	-0.003	0.04
A	HST	limit ₁ –all	0.000	-0.010	-0.005	0.005	0.000	0.010	0.055	0.000	0.06
A	HST	limit ₁ –limit ₂	0.000	0.015	0.005	-0.005	0.000	-0.010	0.000	0.000	0.06
S	VATT	limit ₁ –all	0.003	0.018	0.000	0.055	0.098	-0.273	0.020	0.000	0.06
S	VATT	limit ₁ –limit ₂	-0.003	0.015	0.000	0.000	-0.098	0.143	0.015	0.000	0.06
S	HST	limit ₁ –all	0.000	0.045	0.010	0.010	0.000	-0.160	0.140	0.000	0.25
S	HST	limit ₁ –limit ₂	0.000	-0.015	-0.005	-0.010	0.000	0.160	0.000	0.000	0.25

NOTE. — **Columns:** (1) Measured parameter (C, A, or S). (2) Mean values were determined within *U*, *B*, *V*, and *R* (VATT), or F300W and F814W (HST). (3) Type of difference calculated: "all" is the mean within the filter set described by column 2 of the median CAS parameter within each type-bin for all of the data; "limit₁" is this median when galaxies with S/N < 100 and resolution > 1.00 kpc are rejected; "limit₂" is this median when galaxies with S/N < 75 and resolution > 1.25 kpc are rejected. (4–11) Median CAS parameter difference (as described in column 3) for each galaxy type-bin. (12) Average error on the median CAS parameter differences.

TABLE 3
CONCENTRATION INDEX (C)

ID#	FUV	σ_{FUV}	NUV	σ_{NUV}	F255W	σ_{F255W}	F300W	σ_{F300W}	<i>U</i>	σ_U	<i>B</i>	σ_B	<i>V</i>	σ_V	<i>R</i>	σ_R	F814W	σ_{F814W}
001	2.617 ²	0.756	2.950 ²	0.728	3.722	0.102
002	2.254	0.023	2.346	0.022
003	2.507	0.044	2.720	0.039	2.404	0.051	2.866	0.039
004	2.247	0.025	2.211	0.024
005	2.488 ²	0.126	2.669 ²	0.115	2.581 ²	0.122	2.343 ²	0.154
006	2.487 ²	0.487	2.784 ²	0.489	2.704	0.043	3.164	0.049
007	2.632	0.113	2.652	0.107	2.770	0.110	2.767	0.125
008	2.125 ²	0.116	2.275 ²	0.116	2.512 ²	0.127	2.851 ²	0.122
009	1.801	0.018
010	4.426	0.165	4.242	0.143	4.088	0.147	4.195	0.140
011	1.407	0.015
012	2.848 ²	0.115	2.860 ²	0.106	2.924 ²	0.109	2.937 ²	0.113
013	3.150 ²	0.378	2.852	0.062	3.060	0.064
014	2.489	0.485	2.622	0.448	2.510	0.032	2.490	0.112	2.682	0.105	2.785	0.096	3.341	0.072	2.571	0.026
015	2.373	0.062	2.442	0.064	2.537	0.080	2.528	0.114
016	2.958	0.031
017	3.022	0.096	3.399	0.113	3.816	0.135	3.997	0.147
018	3.101	0.127	3.041	0.127	2.941	0.133	2.603	0.168
019	1.602	0.058	1.665	0.057	1.629	0.057	1.548	0.057
020	2.526	0.106	2.458	0.106	2.595	0.100	2.546	0.101
021	2.133	0.044	2.250	0.042	2.363	0.042	2.420	0.043
022	3.654	0.095	3.488	0.051
023	1.905	0.018	2.760	0.034	2.745	0.032	2.718	0.031	2.681	0.030	1.790	0.017
024	1.970	0.021	2.046	0.020
025	1.974	0.020	2.271	0.023

NOTE. — **Columns:** Concentration indices in each filter and their uncertainties (σ_{filter}). The ID# is the identification number assigned to each galaxy in Table 1. The full table is available only in the electronic edition.

^aGalaxy does not meet the S/N requirements for accurate CAS parameter measurements in this image (S/N < 75).

^bGalaxy does not meet the resolution requirements for accurate CAS parameter measurements in this image (R > 1.25 kpc).

and NUV filters, as well as the HST F255W filter, but the other filters show a trend of decreasing C, and increasing A and S toward later type for normal galaxies (E through Im). The slope of the dependence of A and S on type for normal galaxies decreases toward longer wavelengths, such that late-type galaxies are more asymmetric and clumpy at shorter wavelengths than at longer wavelengths, which is also seen in Figures 4–6. The peculiar/merging galaxies are plotted as their sub-types, as

defined in Section 4.1, in Figures 7–9. Merging galaxies (solid triangles) tend to be in general much less concentrated and much more asymmetric and clumpy than any other galaxy type. Pre-merging galaxies (solid circles) have similar or slightly lower C and higher A and S values than normal mid- to late-type galaxies, because these galaxies are currently only slightly distorted by the tidal interactions with their neighbors. Minor mergers (solid squares) are slightly more concentrated and less asym-

TABLE 4
ASYMMETRY INDEX (A)

ID#	FUV	σ_{FUV}	NUV	σ_{NUV}	F255W	σ_{F255W}	F300W	σ_{F300W}	U	σ_U	B	σ_B	V	σ_V	R	σ_R	F814W	σ_{F814W}
001	0.354 ²	0.022	0.208 ²	0.006	0.292	0.010
002	0.383	0.013	0.180	0.005
003	0.373	0.049	0.368	0.025	0.391	0.018	0.226	0.092
004	0.745	0.005	0.359	0.003
005	0.309 ²	0.069	0.479 ²	0.019	0.371 ²	0.017	0.245 ²	0.043
006	0.635 ²	0.001	0.534 ²	0.001	0.668	0.005	0.293	0.006
007	0.504	0.035	0.541	0.016	0.539	0.011	0.460	0.030
008	0.329 ²	0.034	0.273 ²	0.026	0.271 ²	0.008	0.248 ²	0.006
009	0.264	0.038
010	0.424	0.021	0.416	0.016	0.379	0.009	0.407	0.006
011	0.306	0.013
012	0.448 ²	0.028	0.524 ²	0.004	0.461 ²	0.004	0.444 ²	0.007
013	0.348 ²	0.064	1.480	0.027	0.620	0.004
014	0.380	0.009	0.287	0.005	0.323	0.041	0.235	0.024	0.150	0.036	0.157	0.021	0.171	0.022	0.132	0.018
015	0.211	0.176	0.235	0.118	0.350	0.074	0.073	0.129
016	0.593	0.004
017	0.250	0.008	0.162	0.011	0.132	0.006	0.119	0.004
018	0.287	0.040	0.277	0.014	0.209	0.035	0.158	0.025
019	0.837	0.023	0.956	0.004	0.991	0.003	1.034	0.004
020	0.231	0.095	0.292	0.030	0.266	0.022	0.211	0.041
021	0.268	0.025	0.188	0.021	0.166	0.012	0.156	0.010
022	0.330	0.000	0.132	0.001
023	0.385	0.007	0.402	0.035	0.409	0.008	0.392	0.007	0.373	0.005	0.219	0.003
024	0.341	0.022	0.206	0.008
025	0.605	0.008	0.198	0.002

NOTE. — **Columns:** Asymmetry indices in each filter and their uncertainties (σ_{filter}). The ID# is the identification number assigned to each galaxy in Table 1. The full table is available only in the electronic edition.

^aGalaxy does not meet the S/N requirements for accurate CAS parameter measurements in this image (S/N < 75).

^bGalaxy does not meet the resolution requirements for accurate CAS parameter measurements in this image (R > 1.25 kpc).

TABLE 5
CLUMPINESS INDEX (S)

ID#	FUV	σ_{FUV}	NUV	σ_{NUV}	F255W	σ_{F255W}	F300W	σ_{F300W}	U	σ_U	B	σ_B	V	σ_V	R	σ_R	F814W	σ_{F814W}
001	0.00 ²	0.000	0.00 ²	0.000	-0.01	0.038
002	0.16	0.194	0.25	0.187
003	0.75	0.092	0.44	0.078	0.53	0.057	0.25	0.036
004	0.57	0.256	0.27	0.154
005	0.30 ²	0.041	0.52 ²	0.062	0.51 ²	0.051	0.22 ²	0.026
006	0.53 ²	0.883	0.32 ²	0.380	0.63	0.225	0.37	0.162
007	0.42	0.034	0.43	0.035	0.42	0.032	0.18	0.015
008	0.50 ²	0.037	0.32 ²	0.030	0.32 ²	0.021	0.34 ²	0.017
009	-0.40	0.468
010	0.67	0.019	0.61	0.028	0.53	0.019	0.64	0.018
011	0.50	0.332
012	0.27 ²	0.023	0.40 ²	0.031	0.35 ²	0.022	0.38 ²	0.017
013	0.57 ²	2.095	1.01	0.628	0.32	0.156
014	0.81	1.873	0.28	0.619	0.61	0.448	0.20	0.017	0.15	0.018	0.17	0.016	0.11	0.013	-0.10	0.144
015	0.18	0.048	0.38	0.090	0.44	0.082	-0.84	0.094
016	0.71	0.188
017	0.69	0.030	0.42	0.019	0.32	0.010	0.31	0.007
018	0.58	0.038	0.38	0.034	0.31	0.025	0.08	0.010
019	0.81	0.024	0.99	0.030	0.97	0.023	0.93	0.018
020	0.36	0.037	0.40	0.045	0.38	0.036	0.31	0.027
021	0.68	0.039	0.40	0.034	0.33	0.024	0.31	0.019
022	0.30	0.035	0.35	0.056
023	0.04	0.076	0.75	0.035	0.65	0.038	0.59	0.028	0.56	0.023	0.16	0.132
024	0.51	0.353	0.15	0.162
025	0.77	0.265	0.20	0.104

NOTE. — **Columns:** Clumpiness indices in each filter and their uncertainties (σ_{filter}). The ID# is the identification number assigned to each galaxy in Table 1. The full table is available only in the electronic edition.

^aGalaxy does not meet the S/N requirements for accurate CAS parameter measurements in this image (S/N < 75).

^bGalaxy does not meet the resolution requirements for accurate CAS parameter measurements in this image (R > 1.25 kpc).

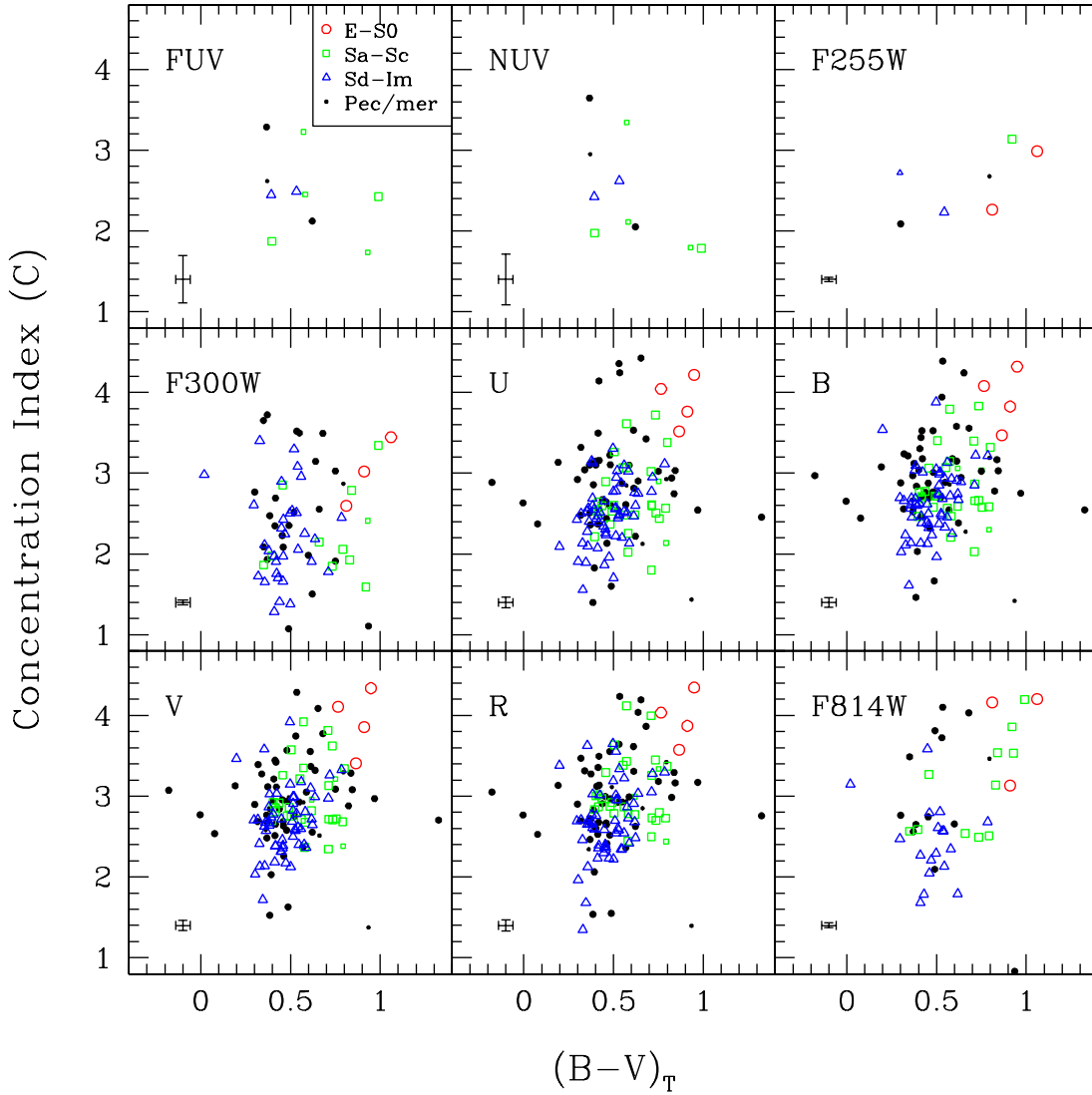


FIG. 4.— Concentration index as a function of total $(B - V)$ color for nine different pass-bands. The symbols are coded by galaxy type, as indicated in the upper left (FUV) panel. Smaller symbols represent galaxies that do not meet our adopted reliability criteria (see text). Vertical error bars in the lower left corner of each panel represent the median error on the individual concentration index values. Horizontal error bars show the median error on $(B - V)$. In general, redder galaxies tend to be more concentrated. This trend also results in a segregation according to galaxy type.

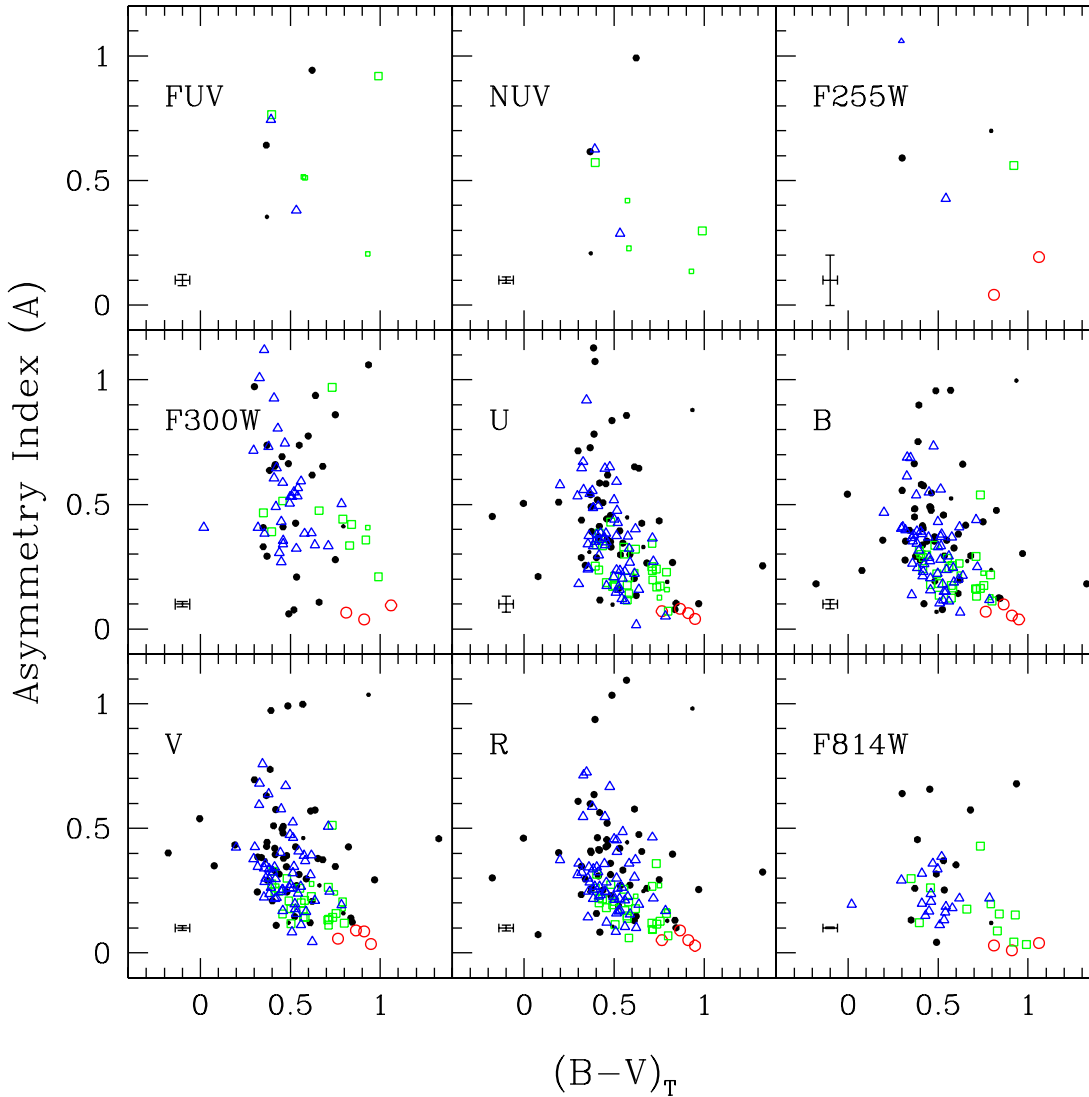


FIG. 5.— Asymmetry index as a function of total $(B - V)$ color and filter. The symbols are coded as in Fig. 4. Error bars in the lower left corner of each panel represent the median error on the individual asymmetry values and on $(B - V)$. In general, redder galaxies tend to be more symmetric. As in Fig. 4, this trend with galaxy color also results in a segregation according to galaxy type. Peculiar/merging galaxies are in general slightly bluer and more asymmetric than normal galaxies.

metric and clumpy than the pre-mergers, because the low mass of the smaller interacting galaxy has likely less of an effect on the brighter, larger galaxy’s light distribution than a neighboring galaxy of similar size would have had. This is also found in minor vs. major merger simulations (Conselice 2006). Merger remnants (asterisks) are more concentrated, more asymmetric, and similar in clumpiness to pre-mergers and normal mid- to late-type galaxies. Peculiar galaxies (crosses) have similar CAS values as normal mid- to late-type galaxies, although they appear slightly more concentrated and more asymmetric in some filters.

Histograms of the distribution of the CAS parameters as separated by galaxy type are presented in Figure 10. These distributions demonstrate the amount of overlap in the CAS parameters between different galaxy type-bins, and therefore are relevant to help judge the reliability

of using these parameters to classify galaxies. The left panels of this plot contain all data in filters with wavelengths shortward of the Balmer break ($\lambda_c \lesssim 360$ nm), and the right panels contain all data in filters with wavelengths longward of the Balmer break ($\lambda_c \gtrsim 360$ nm). Galaxies that did not meet our reliability criteria were not included in this plot. There is a large amount of overlap between the concentration indices of all galaxy types, particularly at shorter wavelengths. Early galaxy types are better separated from other galaxy types by concentration at longer wavelengths, although there is still a significant amount of overlap for smaller values of C . Very few galaxies with types later than S0 have high values of C . Therefore, there is a high probability that a galaxy with high concentration index ($C \gtrsim 3.5$) is an early-type (E–S0) galaxy. Similarly, early-type (E–S0) galaxies have very little overlap with later galaxy types in asymmetry

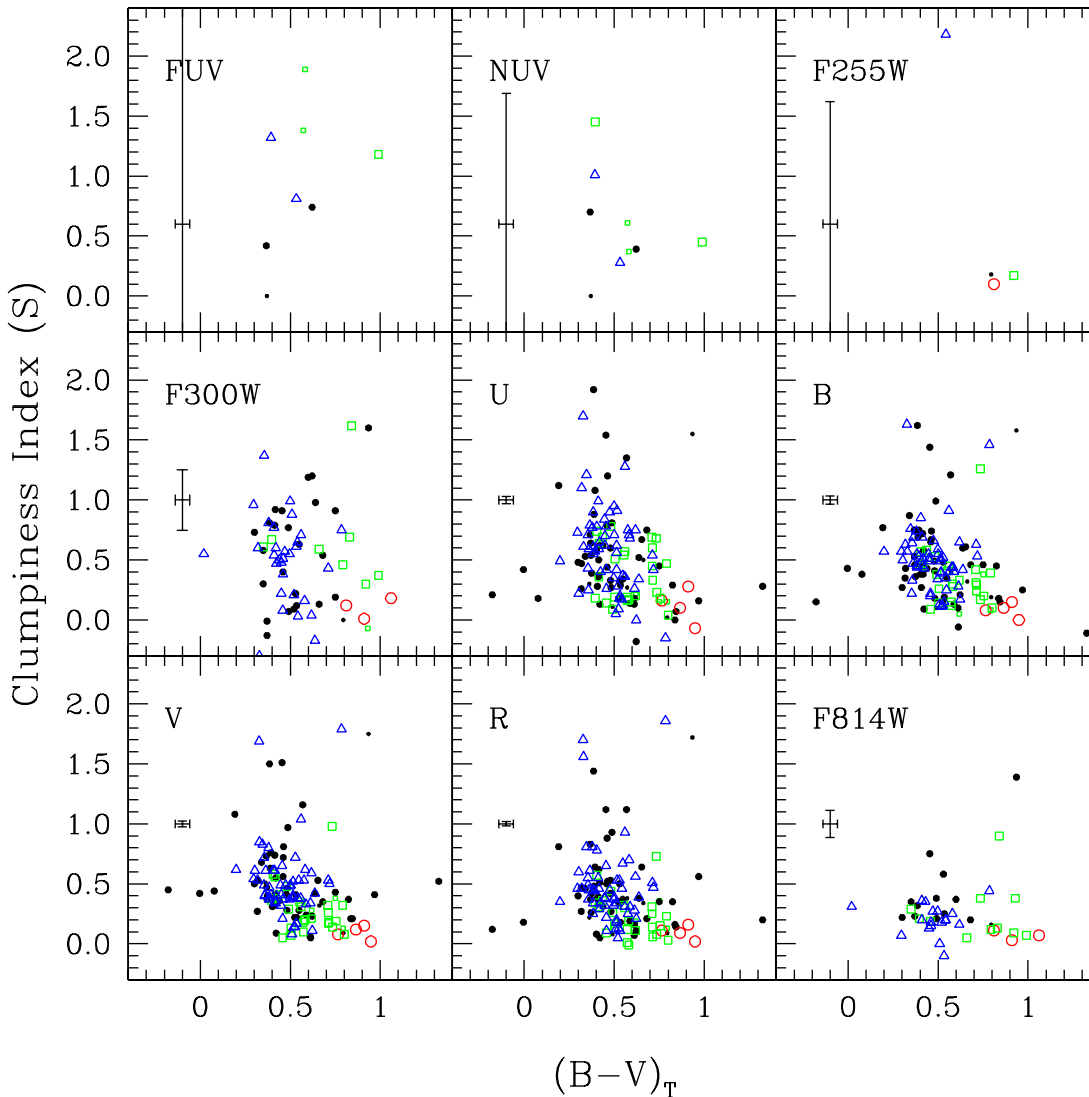


FIG. 6.— Clumpiness index as a function of total $(B - V)$ color and filter. The symbols are coded as in Fig. 4. Error bars on the left side of each panel represent the median error on the individual clumpiness values, and on $(B - V)$. The large errors in S for FUV and NUV are due to the low resolution of the GALEX images (stellar FWHM $\gtrsim 5''$), while the large errors in F255W and F300W are due to poor S/N and CTE effects. In general, redder galaxies tend to be less clumpy. As in Figs. 4 and 5, this trend with galaxy color also results in a segregation according to galaxy type. There is a larger spread in S at shorter wavelengths, with blue galaxies appearing more clumpy at shorter wavelengths than they do at longer wavelengths. Peculiar/merging galaxies are in general slightly bluer and more clumpy than normal galaxies.

index, particularly at longer wavelengths. Galaxies with $A \lesssim 0.1$ are likely early-types (E-S0), which is essentially true at all wavelengths. Although all early-type (E-S0) galaxies have low clumpiness indices, there is a larger overlap with later-type galaxies for this index than for the concentration and asymmetry indices. In general, almost all early-type (E-S0) galaxies have $S \lesssim 0.2$, but not all galaxies with $S \lesssim 0.2$ are early-types. There is a single early-type galaxy with a high S measurement in the NUV, but this is likely due to low S/N in the parts of the galaxy just outside its bright inner core. Although all of the later (Sa-Im and peculiar/merging) galaxy type distributions are offset slightly from each other in mean C , A , and S , there is a large overlap between their CAS parameter values. Therefore, the CAS parameters can-

not be used independently to classify individual galaxies with types later than Sa, but they can be used to describe something about the overall distribution of types as a whole in a large sample. Nonetheless, it is noteworthy that a subset of the peculiar/merging galaxies, predominantly major mergers, display high asymmetry indices at longer wavelengths that are not seen for the other galaxy types. The next two sections discuss using a combination of the CAS parameters as a more reliable way of determining the morphological distributions within a galaxy sample.

6.2. The Distribution of Galaxies in CAS Parameter Space

TABLE 6
MEDIAN C FOR EACH GALAXY TYPE BIN

Type	FUV	NUV	F255W	F300W	<i>U</i>	<i>B</i>	<i>V</i>	<i>R</i>	F814W
E-S0	...	1.73(1)	2.63(2)	2.93(4)	3.90(4)	3.95(4)	3.98(4)	3.95(4)	3.65(4)
	0.36	0.26	0.24	0.28	0.30	0.23	0.55
Sa-Sc	2.15(2)	1.88(2)	3.14(1)	2.06(11)	2.58(26)	2.71(26)	2.84(26)	2.90(26)	3.18(12)
	0.28	0.09	...	0.46	0.25	0.24	0.26	0.28	0.49
Sd-Im	2.47(2)	2.52(2)	2.23(1)	2.11(41)	2.50(55)	2.63(55)	2.67(55)	2.65(55)	2.35(25)
	0.02	0.10	...	0.35	0.26	0.27	0.29	0.32	0.28
pM	2.12(1)	2.05(1)	...	2.22(8)	2.60(7)	2.77(7)	2.58(7)	2.63(7)	2.86(4)
	0.35	0.36	0.36	0.39	0.39	0.53
mM	1.89(1)	1.94(3)	3.03(3)	3.03(3)	3.08(3)	3.17(3)	2.56(3)
	0.79	0.94	0.91	0.81	0.76	1.25
M	2.30(2)	1.44(6)	2.61(3)	2.54(3)	2.37(3)	2.36(3)	1.47(4)
	0.15	0.67	0.63	0.59	0.61	0.64	0.79
MR	3.29(1)	3.65(1)	...	2.69(5)	3.04(15)	3.15(15)	3.21(15)	3.18(15)	3.19(2)
	0.34	0.20	0.26	0.31	0.44	0.54
P	2.09(1)	2.90(8)	2.67(21)	2.88(21)	2.93(21)	2.93(21)	3.13(4)
	0.59	0.28	0.17	0.18	0.22	0.50

NOTE. — Median concentration indices in each type-bin and filter. Galaxies that did not meet the reliability criteria ($S/N < 75$, or $R > 1.25$ kpc) were not included in the median. Values in parenthesis give the number of galaxies used for that type-bin and filter. The second line for each type-bin lists half the range of the data within the 25 and 75% quartiles. When only one data point was available, the value listed is for that data point and the associated quartile range cannot be computed. The peculiar/merging galaxies are broken up into sub-types as follows: pre-merger (pM), minor merger (mM), merger (M), merger remnant (MR), and peculiar (P). In general, C increases with increasing rest-frame wavelength.

TABLE 7
MEDIAN A FOR EACH GALAXY TYPE BIN

Type	FUV	NUV	F255W	F300W	<i>U</i>	<i>B</i>	<i>V</i>	<i>R</i>	F814W
E-S0	...	0.19(1)	0.12(2)	0.08(4)	0.07(4)	0.06(4)	0.07(4)	0.05(4)	0.03(4)
	0.08	0.04	0.01	0.02	0.02	0.02	0.01
Sa-Sc	0.84(2)	0.44(2)	0.56(1)	0.42(11)	0.23(26)	0.22(26)	0.20(26)	0.18(26)	0.15(12)
	0.08	0.14	...	0.07	0.07	0.06	0.06	0.05	0.06
Sd-Im	0.56(2)	0.46(2)	0.43(1)	0.50(41)	0.36(55)	0.32(55)	0.30(55)	0.27(55)	0.22(25)
	0.18	0.17	...	0.11	0.13	0.09	0.08	0.07	0.06
pM	0.94(1)	0.99(1)	...	0.64(8)	0.36(7)	0.34(7)	0.33(7)	0.31(7)	0.34(4)
	0.24	0.16	0.11	0.11	0.13	0.15
mM	0.78(1)	0.74(3)	0.30(3)	0.29(3)	0.27(3)	0.27(3)	0.26(3)
	0.53	0.19	0.18	0.16	0.15	0.43
M	0.80(2)	1.09(6)	0.84(3)	0.96(3)	0.99(3)	1.03(3)	0.84(4)
	0.19	0.14	0.04	0.10	0.13	0.23	0.07
MR	0.64(1)	0.62(1)	...	0.66(5)	0.43(15)	0.43(15)	0.43(15)	0.41(15)	0.41(2)
	0.11	0.15	0.14	0.10	0.13	0.04
P	0.59(1)	0.37(8)	0.36(21)	0.30(21)	0.37(21)	0.30(21)	0.61(4)
	0.19	0.12	0.13	0.10	0.10	0.15

NOTE. — Median asymmetry indices in each type-bin and filter. Galaxies that did not meet the reliability criteria ($S/N < 75$, or $R > 1.25$ kpc) were not included in the median. Values in parenthesis give the number of galaxies used for that type-bin and filter. The second line for each type-bin lists half the range of the data within the 25 and 75% quartiles. Median values that were only calculated from one data point do not have an associated quartile range listed. The peculiar/merging galaxies are broken up into sub-types as follows: pre-merger (pM), minor merger (mM), merger (M), merger remnant (MR), and peculiar (P). In general, A decreases with increasing rest-frame wavelength.

The CAS parameters have been shown to correlate with each other to form parameter spaces that can be used to classify galaxies, distinguish between interacting and merging galaxies, and determine the extent of recent star formation (Conselice 2003). We examine the distribution of the galaxies within our sample in the CAS parameter space by plotting the three parameters against each other in Figures 11–15.

Figure 11 shows the concentration index for each galaxy as a function of asymmetry index and filter. Plot symbols are coded according to galaxy type. In this figure we do not separate the peculiar and merging galax-

ies into their sub-types. Smaller symbols are used for galaxies that did not meet our reliability criteria ($S/N < 75$, $R > 1.25$ kpc). In order to examine the effects of high physical resolution and dust lanes, we also indicate whether galaxies are particularly nearby ($R < 20$ pc), or appear to be edge-on spirals. In general, galaxies become less concentrated toward higher asymmetry, which agrees with the results of other studies (e.g., Conselice 2003). Galaxy types overlap within this plot, but early-type galaxies (E-S0) are in general the most concentrated and the most symmetric, while later galaxy types become in general less concentrated and more asymmet-

TABLE 8
 MEDIAN S FOR EACH GALAXY TYPE BIN

Type	FUV	NUV	F255W	F300W	<i>U</i>	<i>B</i>	<i>V</i>	<i>R</i>	F814W
E-S0	...	2.12(1)	0.10(1)	0.12(3)	0.13(4)	0.09(4)	0.10(4)	0.10(4)	0.05(4)
	0.09	0.10	0.04	0.04	0.04	0.03
Sa-Sc	1.99(2)	0.95(2)	0.17(1)	0.60(10)	0.35(26)	0.32(26)	0.24(26)	0.21(26)	0.16(12)
	0.81	0.50	...	0.17	0.21	0.13	0.10	0.11	0.12
Sd-Im	1.06(2)	0.65(2)	...	0.55(37)	0.59(55)	0.50(55)	0.48(55)	0.44(55)	0.20(25)
	0.26	0.37	...	0.16	0.21	0.10	0.12	0.12	0.06
pM	0.74(1)	0.39(1)	...	0.78(8)	0.36(7)	0.45(7)	0.41(7)	0.37(7)	0.35(4)
	0.38	0.30	0.18	0.12	0.18	0.06
mM	0.12(3)	0.29(3)	0.19(3)	0.22(3)	0.18(3)	0.25(3)
	0.21	0.24	0.15	0.08	0.06	0.11
M	0.94(2)	1.22(6)	0.88(3)	0.99(3)	0.97(3)	0.93(3)	0.75(4)
	0.25	0.32	0.27	0.26	0.27	0.32	0.30
MR	0.42(1)	0.70(1)	...	0.91(5)	0.45(15)	0.46(15)	0.43(15)	0.42(15)	0.45(2)
	0.06	0.19	0.18	0.17	0.15	0.13
P	0.35(8)	0.42(21)	0.38(21)	0.42(21)	0.36(20)	0.29(4)
	0.24	0.18	0.17	0.12	0.15	0.17

NOTE. — Median clumpiness indices in each type-bin and filter. Galaxies that did not meet the reliability criteria ($S/N < 75$, or $R > 1.25$ kpc) were not included in the median, as well as values of $S < -0.2$. Values in parenthesis give the number of galaxies used for that type-bin and filter. The second line for each type-bin lists half the range of the data within the 25 and 75% quartiles. Median values that were only calculated from one data point do not have an associated quartile range listed. The peculiar/merging galaxies are broken up into sub-types as follows: pre-merger (pM), minor merger (mM), merger (M), merger remnant (MR), and peculiar (P). In general, S decreases with increasing rest-frame wavelength.

ric. The merging/peculiar galaxy trend is offset from the normal galaxy trend, with merging/peculiar galaxies (black symbols) tending to be more asymmetric and more concentrated than other galaxy types. The extreme outliers from the general normal galaxy trend tend to be fainter than our S/N limit of 75, and have large associated measurement uncertainties. An edge-on orientation did not have a significant effect on the location of a galaxy within this parameter space. On average, the more nearby galaxies tend to be slightly more asymmetric and less concentrated than their more distant counterparts, which results from their partial resolution into individual stars, as well as a possible selection bias favoring low luminosity dwarf systems at that distance. No systematic trend was noticed in the CAS parameters for galaxies with a physical resolution of $R < 20$ pc.

Figure 12 also shows C vs. A for each galaxy, as in Figure 11, but here the separate sub-classes of peculiar/merging galaxies are represented by different symbols instead of the normal galaxy type-bins. Although there is some overlap, peculiar galaxies tend to be more asymmetric and more concentrated than normal galaxies. For some of these peculiar galaxies, their high concentration in the UV could be due to the presence of an AGN. The pre-mergers tend to be less asymmetric than the other types of mergers, and follow the general trend of normal galaxies except that they are on average slightly more asymmetric. This is to be expected, as the pre-mergers are normal galaxies that are only beginning to be tidally affected by their neighbors, and may show some enhanced star formation. There are very few minor mergers in our sample, with a large scatter in distribution on this plot, so any conclusions about that sub-class should be regarded with caution. We only have four major mergers observed in $UBVR$ in our sample, which is a result of the rarity of these types of galaxies in the

nearby Universe. Although further observations of other mergers are necessary to improve number statistics, most of the major mergers in our sample are clearly separated from the main trend, and are much more asymmetric and less concentrated than any other galaxy type. Merger remnants, on the other hand, lie closer to the trend line for normal galaxies, although they are more asymmetric and more concentrated than both normal galaxies and pre-mergers.

Figure 13 shows the clumpiness index versus the asymmetry index for each galaxy, using the same normal galaxy type symbols as in Figure 11. Measurements of $S < 0$ can occur for particularly smooth or faint galaxies where the sky was measured to be more clumpy than the galaxy itself. This is more likely to occur with HST/WFPC2, due to large noise spikes caused by local CTE effects. The degree to which these S measurements lie below zero is within the uncertainties on S , however. Galaxies tend on average to be more clumpy with higher asymmetry, which agrees with the results of other studies (e.g., Conselice 2003). This relation is fairly tight, especially at longer wavelengths, as S and A are not entirely independent from each other. Early-type galaxies (E-S0) are the least asymmetric and clumpy, with later galaxy types becoming progressively more asymmetric and more clumpy. Outliers from the general trend in the shorter wavelengths have particularly low S/N in the images, while outliers in the longer wavelengths are either edge-on or are very nearby (with resolution, $R < 20$ pc). Due to the strong dust lanes visible in edge-on galaxies, they appear more clumpy than galaxies with lower inclinations, and lie well above the general S vs. A relation. On the whole, nearby galaxies tend to appear to be only slightly more asymmetric and clumpy than their more distant counterparts.

Figure 14 also shows S vs. A for each galaxy, but with

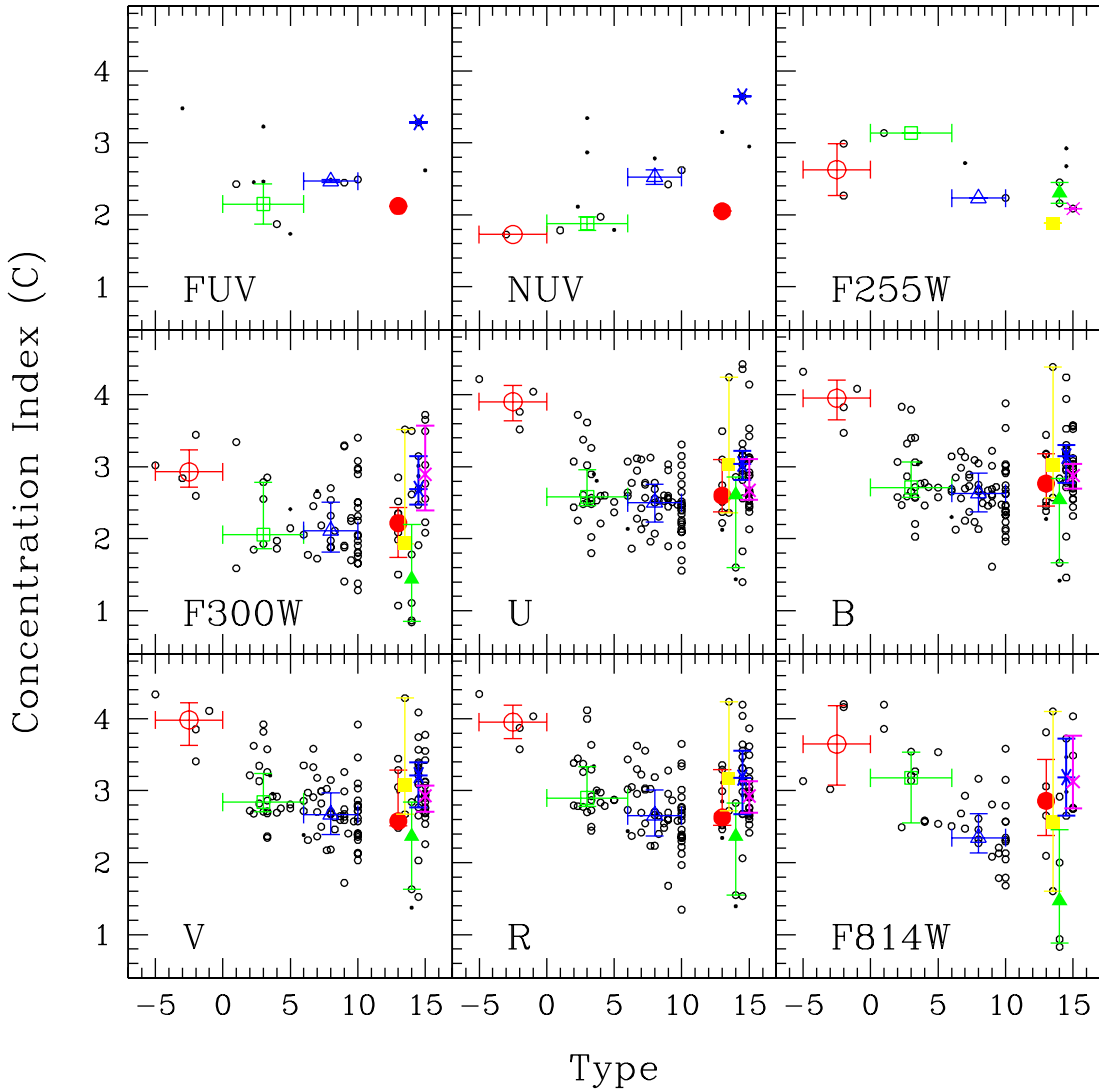


FIG. 7.— Concentration index as a function of galaxy type and filter. Small points represent galaxies that do not meet our adopted reliability criteria (see text). The large colored symbols represent the median C values for a type-bin whose width is defined by the horizontal error bars. The vertical error bars show the 25–75% quartile ranges. These same symbols are used in subsequent figures to represent these galaxy types (as labeled in Fig. 15). There is a larger spread in C with later galaxy type, with galaxies tending on average to be less concentrated with later normal galaxy type (E through Im). Merging galaxies ($T = 14$) are in general less concentrated than all other galaxy types.

peculiar/merging sub-classes highlighted with different symbols, as in Figure 12. The pre-mergers are not clearly distinguished from normal galaxy types within the measurement uncertainties, but merging galaxies are much more asymmetric and show much more small scale structure (clumpiness) than any other galaxy type. Merger remnants tend to appear slightly smoother, but more asymmetric on average than the pre-merger and normal galaxies.

In Figure 15, we examine the average trends in this CAS parameter space with a plot of the average of the median values in each type-bin and filter of C and S as a function of A . The left panels contain the average of the median values in each filter shortward of the Balmer break ($\lambda_c \lesssim 360$ nm). The right panels contain the average of the median values in each filter longward of the

Balmer break ($\lambda_c \gtrsim 360$ nm). Galaxies that did not meet our reliability criteria were not included in the medians. Type-bins in each filter with fewer than 2 galaxies were not used in the average. The error bars are not the errors on the averages, but rather the average value of the 25–75% quartile ranges for each filter used to calculate the average. Therefore, the error bars give an indication of how much an individual galaxy may vary in this parameter space from the average value. There is a much larger scatter in the CAS parameters at shorter wavelengths, which may partially be due to larger measurement uncertainties for these filters and smaller number statistics. More, and higher quality data in the mid to far-UV is needed to further constrain these values. There is a clear trend among normal galaxies to show a progression from early to late-type galaxies (E to Im)

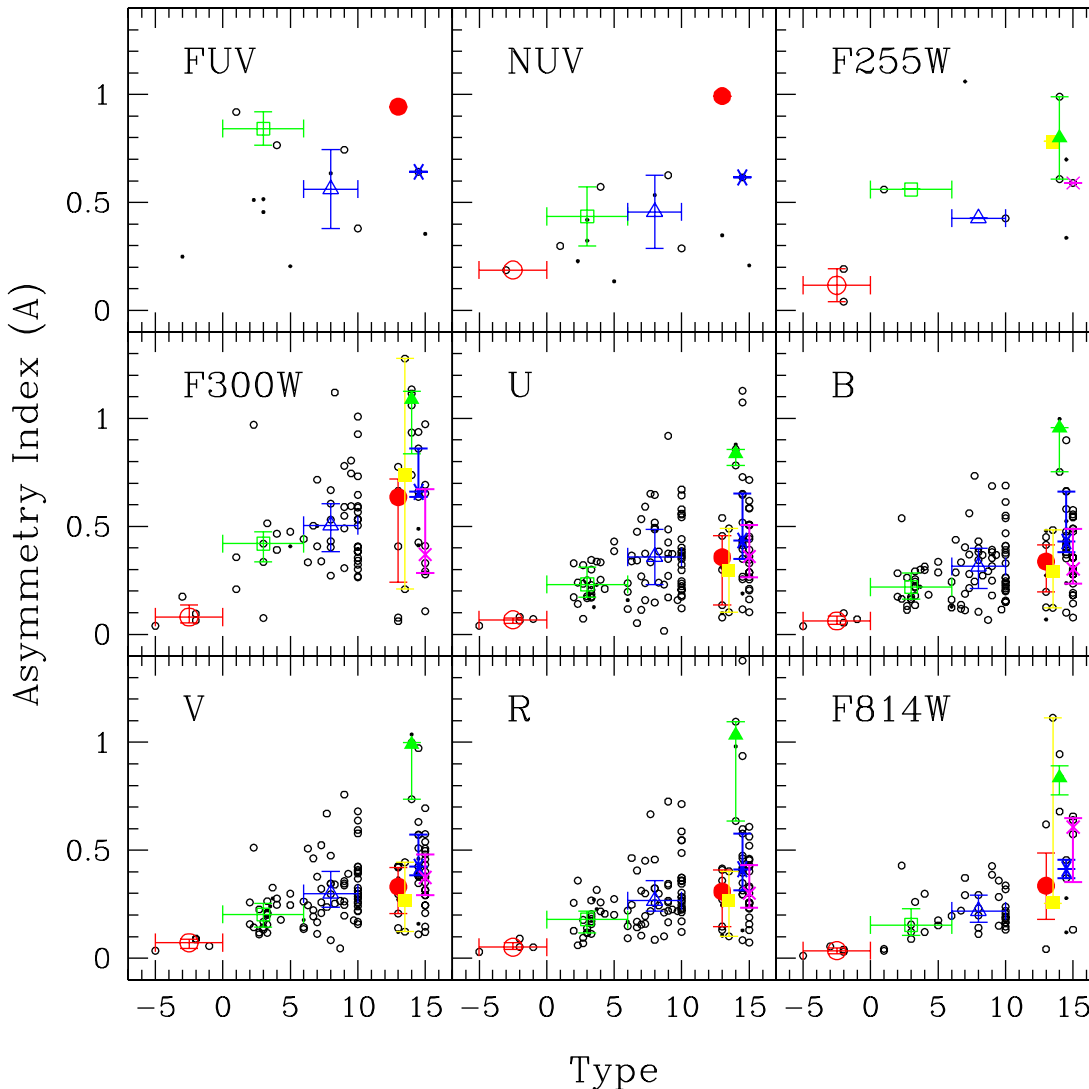


FIG. 8.— Asymmetry index as a function of galaxy type. Symbols are coded as in Fig. 7. The large colored symbols represent the median A values for each galaxy type bin, with error bar as in Fig. 7. There is a larger spread in A for later galaxy types, with galaxies tending on average to be less symmetric with later normal galaxy type (E through Im). Late-type galaxies are less symmetric at shorter wavelengths than at longer wavelengths. Merging galaxies ($T = 14$) are in general less symmetric than all other galaxy types.

of increasing asymmetry and clumpiness and decreasing concentration, particularly in the redder filters. The different peculiar/merging galaxy types are each located at different positions within this parameter space. There appears to be a general evolutionary trend from pre-mergers to mergers, and then to post-mergers, as shown by the dotted lines with arrows connecting the average of the median values for each type-bin. Mergers become significantly less concentrated, more asymmetric, and more clumpy than pre-mergers, then progress back toward the normal galaxy parameter space as they turn into merger remnants, which end up being more concentrated than the pre-mergers, and slightly more asymmetric and clumpy. From there, galaxies may take different paths on the CAS parameter space depending on whether they turn into elliptical or spiral galaxies, which depends on the details of the merger and of the individual galaxies

taking part in that merger.

6.3. Quantitative Classification Using CAS in the Optical and Ultraviolet

One of the major goals of quantitative morphological studies is to automatically distinguish galaxy types from each other. This has proven to be a difficult problem, and various pieces of information, such as colors, magnitude and sizes, are needed in addition to the CAS parameters to fully classify galaxies into various Hubble types automatically. No perfect method has yet been developed. We can however determine how well basic CAS classification boundaries do in terms of automatically finding galaxies of various types, without any other information involved.

A revised CAS classification space can be defined as follows for finding galaxies with early, mid, late and

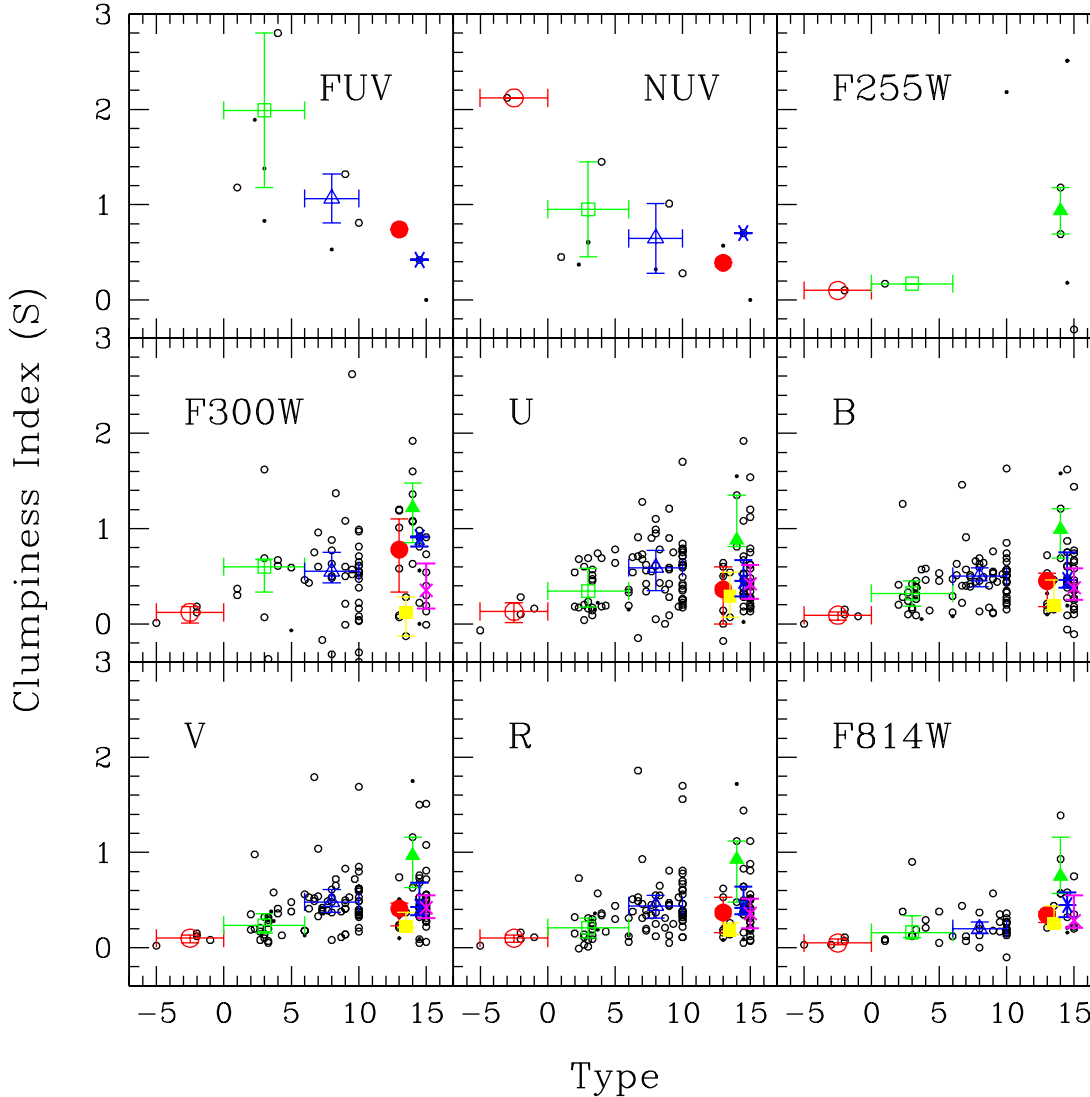


FIG. 9.— Clumpiness index as a function of galaxy type. Symbols are coded as in Fig. 7. The large colored symbols represent the median S values for each type bin, with error bars as in Fig. 7. An additional criteria that $S > -0.2$ was used in the calculation of the median value. There is a larger spread in S with later galaxy type, with galaxies tending on average to be more clumpy with later normal galaxy type (E through Im). Late-type galaxies are more clumpy at shorter wavelengths than at longer wavelengths. Merging galaxies ($T = 14$) are in general more clumpy than any other galaxy type.

merger/peculiar morphologies in rest-frame optical images (see Bershadsky et al. 2000). Early-types are systems with $A < 0.1$ and typically $C > 3.5$, mid-types are those with $0.1 < A < 0.35$ and $C > 2.44 \times \log A + 5.49$, late types with $0.1 < A < 0.35$ and $C < 2.44 \times \log A + 5.49$, and finally mergers have $A > 0.35$ and $A > S$ (Conselice et al. 2004). To carry out the CAS reliability test we examined the position in CAS space of each morphology type to determine what fraction of eye-ball estimates of morphology match the CAS classification boundaries, that is the fraction that are correctly matched (f_{correct}). We also measure the fraction of galaxies within each CAS type volume which do not belong to the assigned type, which we call the contamination fraction (f_{cont}). We remove the nearby galaxies from this analysis to avoid resolution issues.

It turns out that the best results are within the optical region, where the CAS system was originally designed to work. We find that for early-types, $f_{\text{correct}} \sim 1$ in the $UBVR$ and F814W bands. The F225W, NUV and FUV bands only have a few early-types which are too faint for a reliable CAS measurement, but their asymmetry values tend to be a bit higher. The contamination is also very low with $f_{\text{cont}} = 0$ for early-types in the $UBVR$ bands. Most of the contamination in the optical within the $A < 0.1$ CAS space is largely due to mid-types. However, we only have a few early-types and mid-types in our sample, and we are mainly interested in distinguishing late-types from mergers/peculiar, as these galaxies dominate the high redshift population.

The separation of mergers from late-type galaxies can be successfully done within CAS space, although there

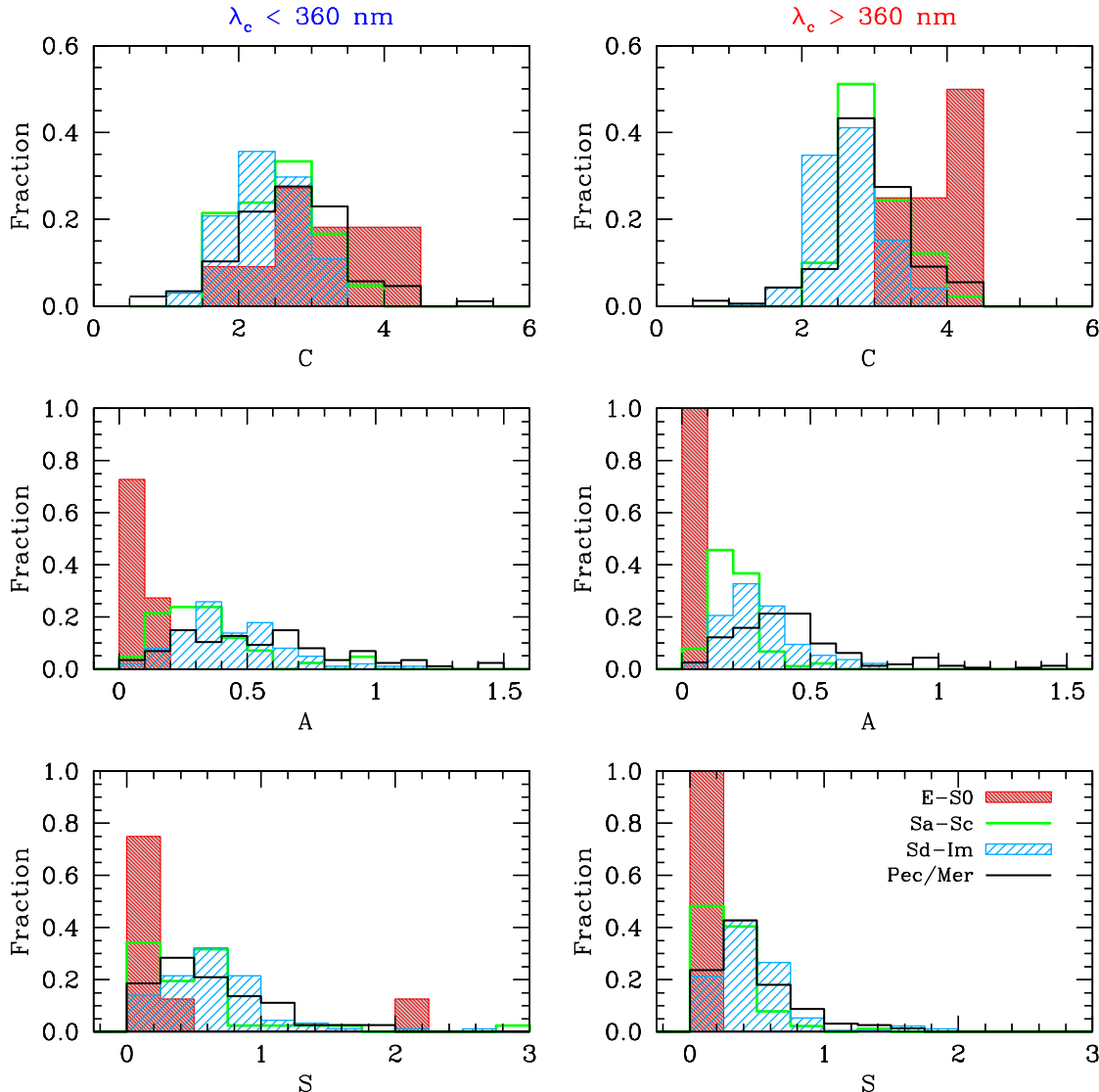


FIG. 10.— The distribution of C (upper panels), A (middle panels), and S (lower panels) for each galaxy type-bin as denoted in the legend in the lower right panel. The left panels include all UV data from all filters shortward of the Balmer break ($\lambda_c \lesssim 360$ nm), and the right panels include all data from all filters longward of the Balmer break ($\lambda_c \gtrsim 360$ nm). Data that did not meet our reliability criteria were not included in this plot. Early-type galaxies (E–S0) have the least amount of overlap with other galaxy types, particularly in longer wavelengths, and particularly in A and S. Galaxies of type Sa and later, however, have considerable overlap in the CAS parameters, although their distributions are offset from each other. Asymmetry and clumpiness can therefore be used independently to classify individual early-type galaxies (E–S0) with some limited degree of certainty, but not individual later-type galaxies. The overall distribution of the CAS parameter in a large sample, however, can be used to describe the population distribution as a whole.

is some overlap. The particular problem, first stated in Conselice (2003), is that not all peculiar/mergers follow the CAS space definition of high asymmetry. Conselice (2003) made this conclusion based on the location of 66 Ultra-Luminous Infrared Galaxies (ULIRGs) in CAS space. About half met the criteria $A > 0.35$, while the remainder were at lower asymmetry, with the systems spread out amongst the concentration index. Using the standard criteria listed above, we find that for late-types, $f_{\text{correct}} \sim 0.5 - 0.9$ in the *UBVR* and F814W bands, with the lowest fraction $f_{\text{correct}} = 0.5$ for the U band, and the highest $f_{\text{correct}} \sim 0.9$ in F814W. Using the same CAS criteria for finding late-types, we find that the contamination ranges from 50% in the U-band, to 20% in the

F814W band, and about 40% in the *BVR* bands. A large part of this contamination arises from peculiar and merging galaxies, which have similar asymmetries. However 70% of galaxies in the late-type regime are classified as late-type by eye, which is a reasonable success rate.

The fraction of mergers found with the basic CAS criteria is not as high, with $f_{\text{correct}} \sim 0.3 - 0.4$ in the *UBVR* bands, and 0.6 in the F814W band. The contamination is also fairly low, with $f_{\text{cont}} \sim 0.2$. This result shows that while most galaxies with a high asymmetry in the *UBRI* bands will be mergers/peculiar, not all mergers/peculiar have large asymmetries (see Conselice 2003). Likewise, some high-A galaxies, particularly in the bluer bands are not classified as a merger or peculiar.

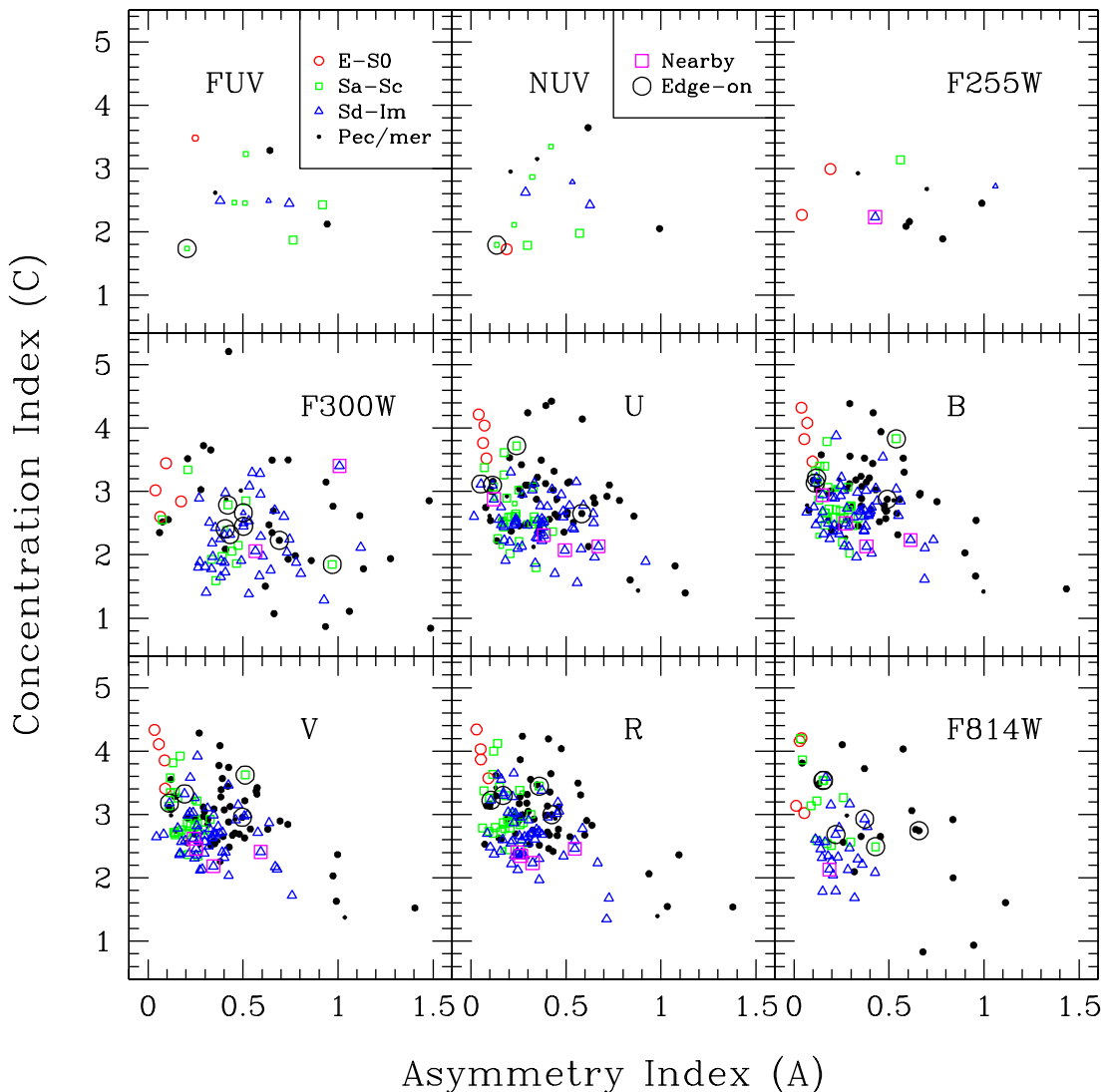


FIG. 11.— Concentration index as a function of asymmetry index and filter. Small points represent galaxies that do not meet our adopted reliability criteria (see text). Plot symbols are coded according to galaxy type as indicated in the legend in the upper left (FUV) panel. Here, we do not separate the peculiar and merging galaxies into their sub-types. We furthermore highlight nearby galaxies in images with particularly high resolutions ($R < 20$ pc), as well as highly inclined/edge-on galaxies, by over-plotting larger symbols coded according to the legend in the upper-middle (NUV) panel. In general, galaxies are less concentrated when they are less symmetric. Increasingly later galaxy types become increasingly less concentrated and more asymmetric. The locus of merging/peculiar galaxies is offset from that of the normal galaxies toward higher asymmetries and concentrations. Extreme outliers from the general trend are usually fainter than our S/N limit of 75, and have large associated measurement uncertainties. Particularly nearby galaxies, which tend to be partially resolved into their individual stars, are on average slightly less symmetric and less concentrated than more distant galaxies, due in part to spatial resolution effects.

It is worth noting that the best results are obtained using the reddest band, F814W, which suggests that measurements of galaxy structure are best done in the reddest wave-band possible.

A major goal of this paper is to test whether we can tell the difference between late-type star forming galaxies and mergers through the CAS parameters in the ultraviolet. It turns out that the ability to distinguish late-types from mergers/peculiar is slightly worse in the UV than in the optical, but not by much. Using the standard CAS method, 50% of eye-ball classified late-types fall in their correct CAS region in the NUV. The late-types in the UV which do not fall in the correct UV-CAS region typically

have high asymmetries, $A > 0.35$ (Figure 11). Generally, these galaxies have high clumpiness values as well. We can use this fact to better automatically separate late-type galaxies from mergers/peculiar in the ultraviolet. If we take the following criteria:

$$A > 0.25 \text{ and } C < 2.44 \times \log A + 5.49 \text{ and } S > A, \quad (4)$$

we acquire 60% of the late-types, with a 40% contamination rate from mostly peculiar/mergers in the F300W and U-bands. This contamination is again largely the result of peculiar/mergers.

Using the standard revised optical CAS method for

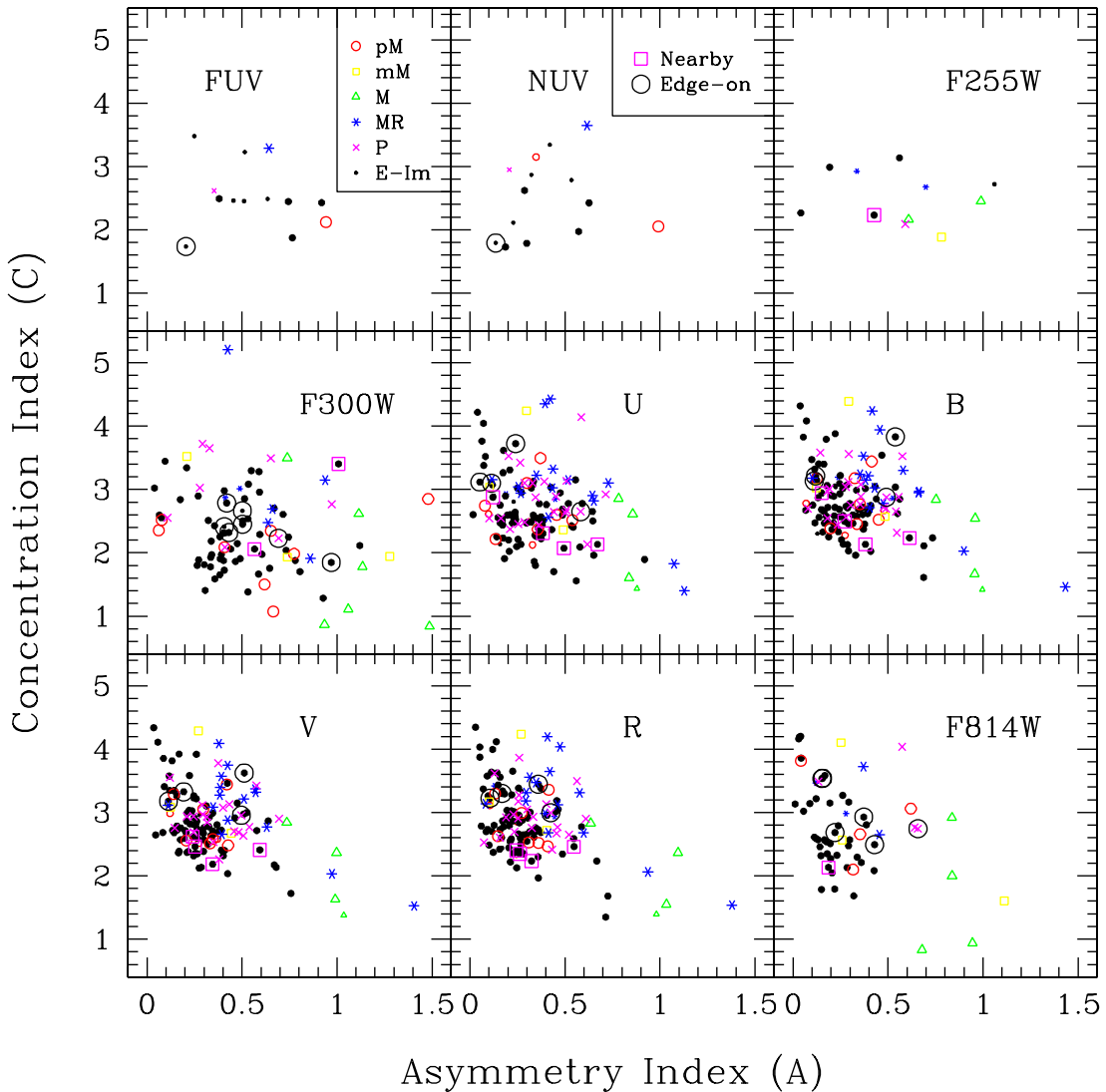


FIG. 12.— Concentration index vs. asymmetry index, as in Fig. 11, but with plot highlighting the individual sub-classes of merging and peculiar galaxies rather than normal morphological types. Peculiar galaxies (P) are on average less symmetric and more concentrated than normal galaxies. For some of these peculiar galaxies, their high concentration in the UV could be due to the presence of an AGN. Pre-mergers (pM) tend to be slightly less symmetric than normal galaxies. Major mergers (M) are much less symmetric and less concentrated than any other galaxy type. Merger remnants (MR) are less symmetric and more concentrated than both normal galaxies and pre-mergers.

finding mergers ($A > 0.35$ and $A > S$) we find that all mergers/peculiar galaxies are identified in the FUV, 50% in the NUV, 75% in the F225W band and 40% in the F300W band. The contamination rates within the area of CAS for mergers in the FUV, NUV, F225W and F300W are 0%, 0%, 25%, and 33% respectively. It is clear from Figures 11–14 that the asymmetry limit of $A > 0.35$ has a contamination from late-type galaxies. This is due to the increased prominence of star formation in the UV, creating high asymmetries which are sensitive to star formation and merging activity (Conselice et al. 2000). However, if we increase the limit to $A = 0.6$ in the UV, we are able to obtain a nearly clean sample of mergers. This new UV-CAS criteria for finding mergers is:

$$A > 0.5 \text{ and } A > S. \quad (5)$$

Using equation (5) to find mergers in the F300W band we get $f_{\text{correct}} \sim 0.4$, while $f_{\text{con}} = 0.25$. In the F255W band the contamination is also low, $f_{\text{con}} = 0.25$, and the $f_{\text{correct}} \sim 0.75$, although there are too few merging galaxies (3) in this pass-band to draw definite conclusions. The NUV and FUV bands have too few galaxies to reliably compute these statistics. We suggest that future studies that use rest-frame UV morphologies of high redshift galaxies use the UV-CAS equations (4–5) to separate late-types from mergers, although larger number statistics in the UV are needed to verify these results.

6.4. The Rest-frame Wavelength Dependence of the CAS Parameters.

Some of the galaxies in our sample appear different in the UV than they do in the optical, while some galax-

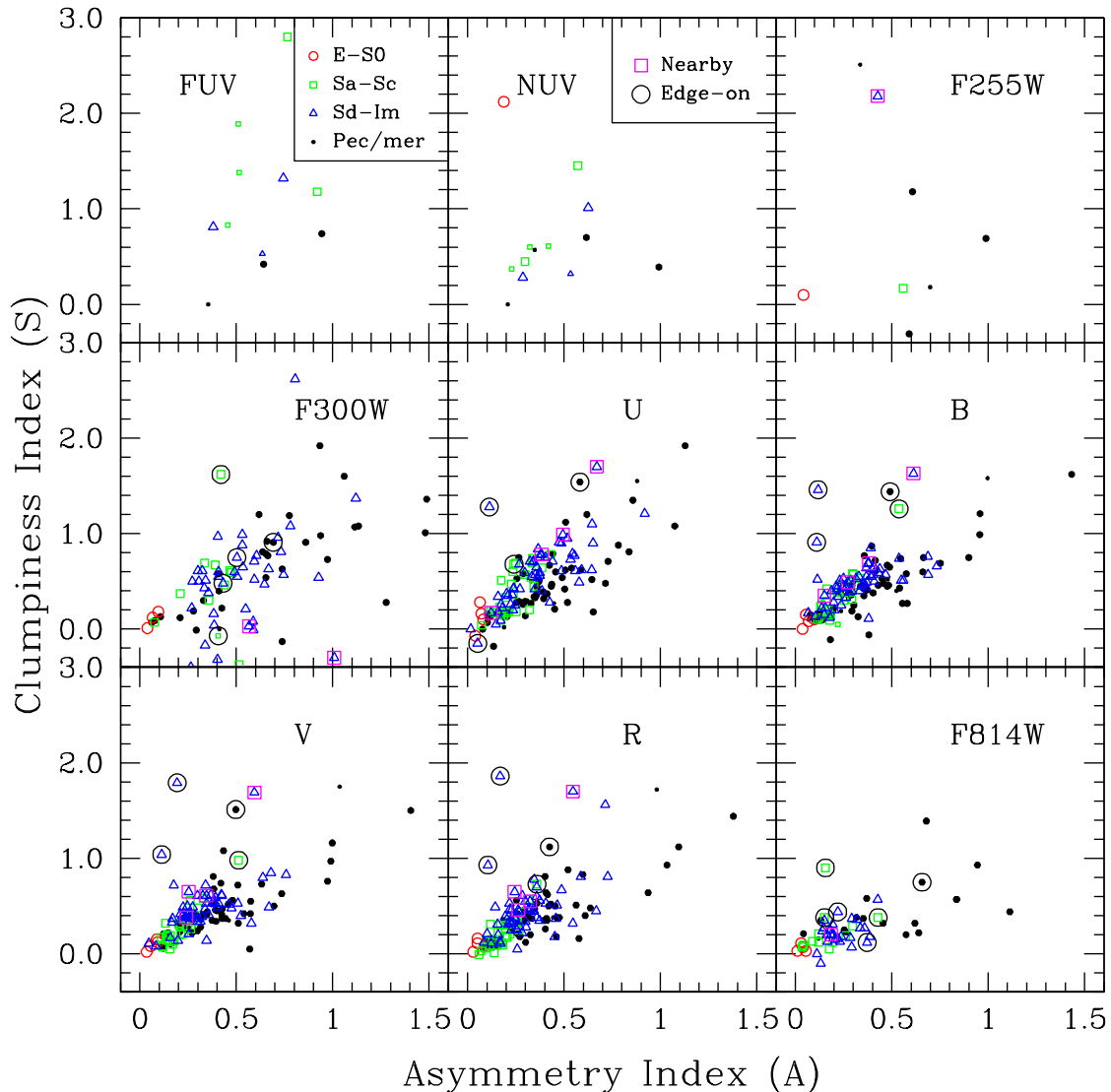


FIG. 13.— Clumpiness index vs. asymmetry index. Symbols are coded as in Fig. 11. Galaxies are on average more clumpy when they are less symmetric. Increasingly later galaxy types become progressively less symmetric and more clumpy. Outliers in the shorter wavelengths tend to have $S/N < 75$, and large associated uncertainties. Edge-on spirals are well separated from the general trend, appearing more clumpy than galaxies with lower inclinations. This is likely due to more visible dust-lanes that increase the clumpiness index. Particularly nearby galaxies tend to be slightly less symmetric and more clumpy than more distant galaxies, due to resolution effects.

ies appear very similar. This was discussed qualitatively in detail in Windhorst et al. (2002). Figure 16 shows examples of each of these cases. The upper image for each galaxy was obtained with either the F814W near-IR filter, or the VATT R-band filter. The lower image for each galaxy was obtained with either the F300W UV filter, or the VATT U-band filter. UGC05189 is a merger remnant that has a large difference in asymmetries and clumpiness indices between the UV and the IR ($A_{F300W} - A_{F814W} = 0.182$, and $S_{F300W} - S_{F814W} = 0.49$), mostly due to bright star-forming knots that are more apparent in the UV image. UGC06816 is a late-type barred spiral galaxy that has a large difference in A and S between the near-UV and the red ($A_U - A_R = 0.323$, and $S_U - S_R = 0.64$), which is also due to its UV-bright star-forming knots, particularly at the ends of its bar and at two sites

of vigorous star formation along its poorly organized spiral pattern. Both of these galaxies have small differences in concentration index between these filters (-0.178 for UGC05189, and -0.207 for UGC06816). UGC12808 is an earlier-type spiral galaxy that has about the same asymmetry and clumpiness index in both pass-bands ($A_{F300W} - A_{F814W} = -0.045$, and $S_{F300W} - S_{F814W} = -0.05$). UGC06697 is a peculiar, highly inclined galaxy that also has about the same asymmetry and clumpiness index in both pass-bands ($A_{F300W} - A_{F814W} = 0.035$, and $S_{F300W} - S_{F814W} = 0.16$). Both of these galaxies, however, appear different in the UV than in the IR due to a large difference in concentration index between the filters (-0.664 for UGC12808 and -0.515 for UGC06697), which is largely due to the diminished appearance of their red bulges at shorter wavelengths. A quantitative discussion

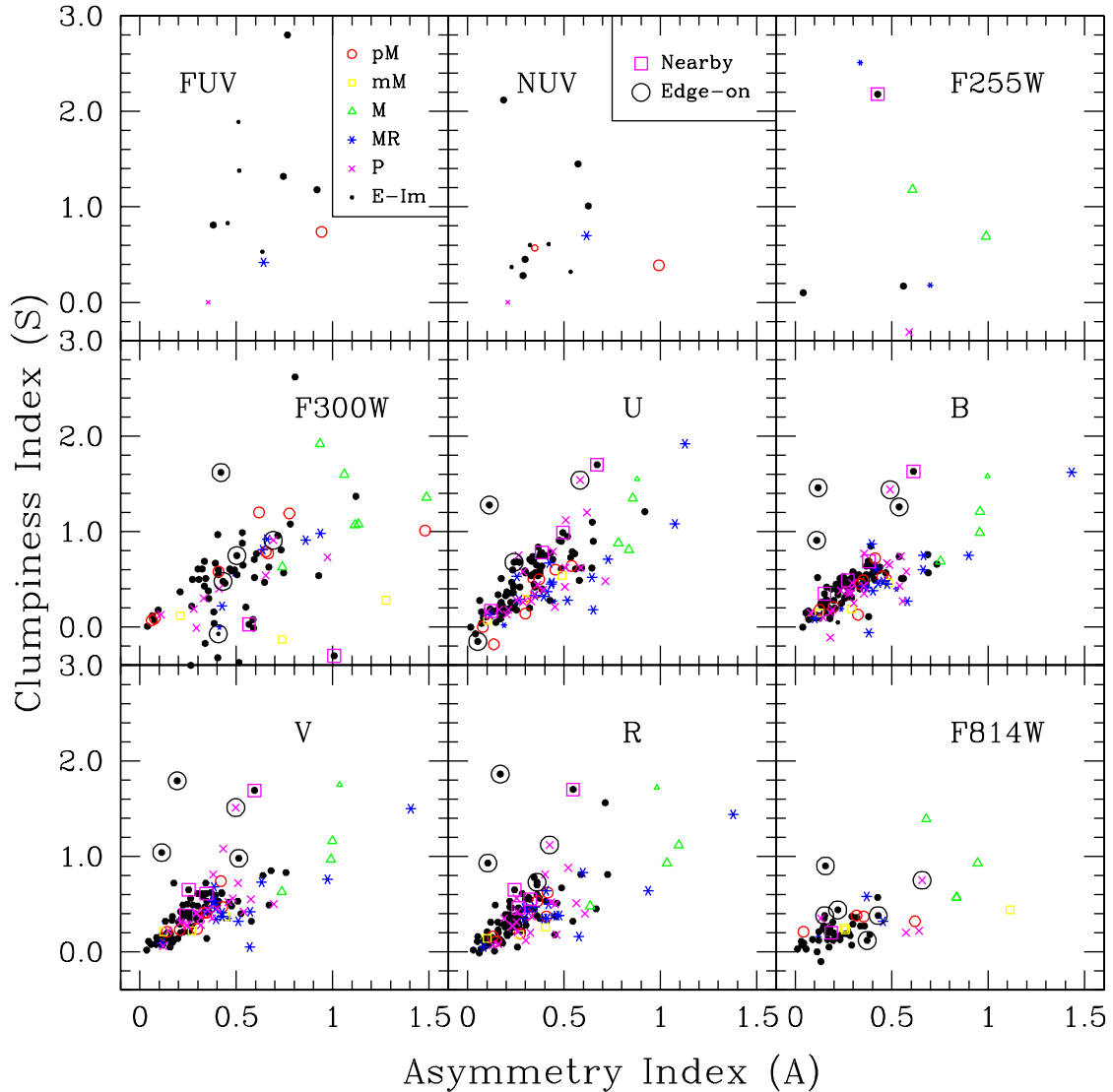


FIG. 14.— Clumpiness index vs. asymmetry index, with merging and peculiar galaxies separated into their sub-classes. Symbols are coded as in Fig. 12. Merging galaxies are much less symmetric and more clumpy than any other galaxy type. Merger remnants tend to be slightly less clumpy and less symmetric than both pre-mergers and normal galaxies.

of the dependence of the CAS parameters on rest-frame wavelength and galaxy type could serve as a zero-redshift benchmark for higher redshift galaxy classifications. As such, we present the results for our dataset below.

Figure 17 shows the median values of the CAS parameters for each type-bin as a function of the central wavelength (λ_c) of each filter in nm. Values of the CAS parameters that were < -0.2 were not included in the median, as well as values from galaxy images that did not meet our reliability criteria. We do not include medians in this plot for filters and type-bins that have fewer than 2 galaxies. Error bars that are the same color as the data points indicate the 25–75% quartile range. Magenta error bars indicate the error on the median, which is smaller for bins that contain larger number statistics. We find a large scatter among individual galaxies, but there is a general trend of increasing C and decreasing A and S toward longer wavelengths. As in previ-

ous plots of the CAS parameters, on average, the early-type, late-type, and merging/peculiar galaxy classes are clearly separated in C, A, and S, although there is considerable overlap among individual galaxies within each type class. The CAS values of early-type galaxies (E–S0) are relatively constant with increasing rest-frame wavelength longward of the Balmer break. Shortward of the Balmer break, the S/N of these red objects is very low, and therefore the CAS parameter measurement uncertainties are high. Due to this effect and due to the lower number of early-type galaxies in our sample, we cannot draw definite conclusions about whether the CAS parameters of early-type galaxies would differ significantly at UV rest-frame wavelengths. Spiral, irregular, and peculiar/merging galaxies, however, all show a general trend of increasing C and decreasing S and A with increasing rest-frame wavelength. The concentrations measured in the HST/WFPC2 F814W images appear somewhat

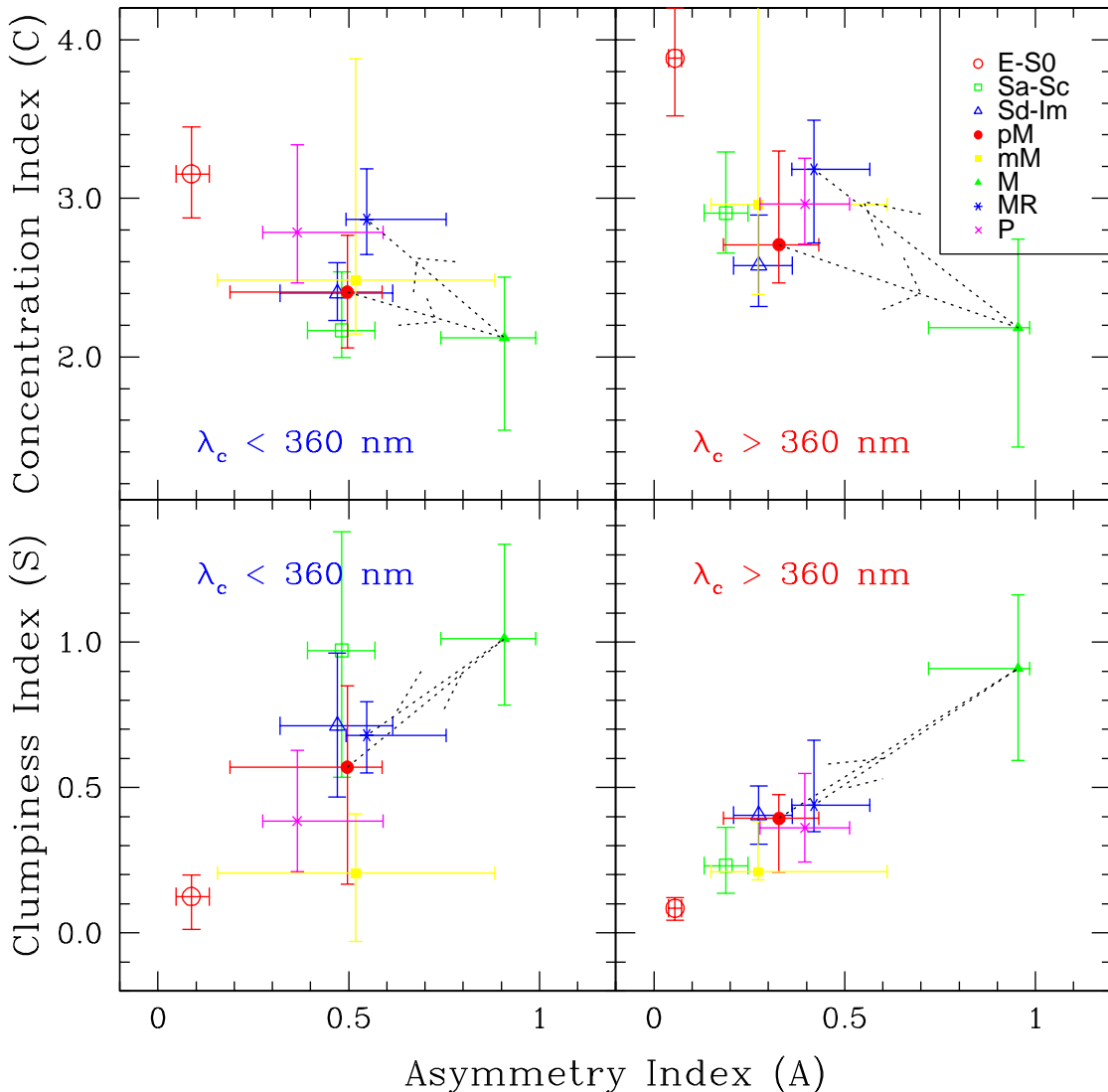


FIG. 15.— The median values of the concentration and clumpiness indices for each type bin vs. the median values of the asymmetry index in that type-bin. Symbols are coded by type as described in the upper right panel. *Left panels:* The average of the median values in each filter short-ward of the Balmer break ($\lambda_c \lesssim 360$ nm). *Right panels:* The average of the median values in each filter long-ward of the Balmer break ($\lambda_c \gtrsim 360$ nm). Galaxies that did not meet our reliability criteria were not included in the medians. Type-bins in each filter with fewer than 2 galaxies were not used in the average. The error bars show the 25–75% quartile ranges of the CAS parameters, averaged over each filter used in the average. There is a larger scatter in the CAS parameters at shorter wavelengths, which may partially be due to lower galaxy number statistics and lower S/N ratio within the GALEX and HST UV images. Normal galaxies become more asymmetric and clumpy and less concentrated toward later Hubble type (E to Im). Dotted lines connect the average of the medians for pre-mergers to mergers, and then to post-mergers. This shows a progression through the CAS parameter space as the merging process progresses, with mergers becoming significantly less concentrated, more asymmetric, and more clumpy than pre-mergers, before returning as post-mergers near the locus of normal galaxies again. On average the merger remnants are more concentrated than the pre-mergers, and slightly more asymmetric and clumpy. This may define a duty cycle for the merging process.

lower with respect to the general trend, which may be due to the fact that our WFPC2 images are more sensitive to point-sources than extended sources, so that outlying low surface-brightness material may not have been detected in that particular filter.

Also, in Figure 17, linear-least-squares fits to the median data points are shown as dashed lines. Linear fits appear suitable for all but the wavelength dependence of the concentration index of early-type (E-S0) galaxies (which shows more sharply decreasing C measurements at wavelengths shortward of the Balmer break), and the

asymmetry and clumpiness indices of mid-type (Sa-Sc) galaxies (which show more sharply increasing A and S measurements shortward of the Balmer break). Therefore, we also include a 2nd order polynomial fit to the data in these panels, shown as dotted lines. This strong dependence of C shortward of the Balmer break for the E-S0 galaxies may be mostly due to the very low S/N of these red galaxies in the UV images (see Windhorst et al. 2002 for the images). This 2nd order polynomial is given by:

$$C(E-S0) = -14.33 \log(\lambda_c)^2 + 78.21 \log(\lambda_c) - 102.6 \quad (6)$$

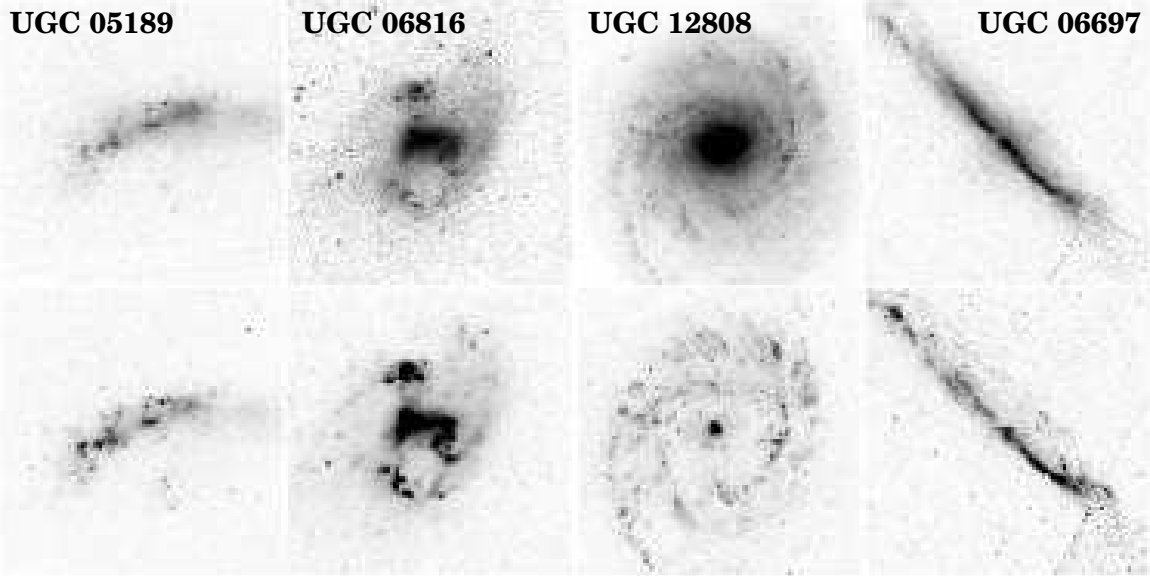


FIG. 16.— Examples of galaxies that have various differences in the CAS parameters as measured in the UV vs. the optical/near-IR. The upper panels are the red (R-band) or near-IR (F814W) images for each galaxy. The lower panels are the UV (U-band or F300W) images for these galaxies. From left to right: UGC05189 is a merger remnant with a large difference in A and S between the UV and the near-IR, but little difference in C. UGC06816 is a late-type spiral galaxy that also has a large difference in A and S between the near-UV and the red, but little difference in C. UGC12808 (NGC7769) is an early-type spiral galaxy that has little difference in A and S between the UV and the near-IR, but a large difference in C. UGC06697 is a peculiar galaxy that also has little difference in A and S between the UV and the near-IR, but a large difference in C. See the text for the differences in CAS parameters for each of these galaxies.

This is a relatively good fit to the data, with 13% uncertainty on each of the coefficients (compared to a 39% error on the slope of the linear fit, and an error larger than the value of the y-intercept). The strong dependence of A and S shortward of the Balmer break for the Sa–Sc galaxies may be due to UV-bright star-forming regions, although the low number statistics in the bluest two filters (2 galaxies) and the large uncertainties suggest that this may be insignificant. However, the general trend of larger A and S values at shorter wavelengths is likely real, as the F300W filter contains 11 Sa–Sc galaxies, and also shows this trend. More far-UV data is needed to more accurately determine the trend in this wavelength range. The 2nd order polynomials for the dependence of A and S on wavelength for Sa–Sc galaxies are:

$$A(Sa - Sc) = 1.69 \log(\lambda_c)^2 - 9.48 \log(\lambda_c) + 13.47 \quad (7)$$

$$S(Sa - Sc) = 5.20 \log(\lambda_c)^2 - 28.82 \log(\lambda_c) + 40.11 \quad (8)$$

The uncertainties on these coefficients are $\lesssim 18\%$, and $\lesssim 10\%$, respectively, compared to an error on the slope of the linear fits of 17% and 18%, respectively.

The coefficients for the linear-least-squares fit are given in Table 9, where $X = X_1 \times \log(\lambda_c) + X_2$, and where λ_c is in units of nm. The variable X is the concentration index (C for columns 2–3), the asymmetry index (A for columns 4–5), or the clumpiness index (S for columns 6–7). As determined from these fits, the early to mid-type spiral galaxies (Sa–Sc) show a significant increase in concentration index at longer rest-frame wavelengths. The late-type (Sd–Im) galaxies, however, have no trend with wavelength within the uncertainties, and there is only a slight trend with wavelength for peculiar/merging galaxies. There is, however, a significant decrease in asymmetry toward longer wavelengths for all galaxy types. The

TABLE 9
CAS WAVELENGTH DEPENDENCE

Type-bin (1)	C ₁ (2)	C ₂ (3)	A ₁ (4)	A ₂ (5)	S ₁ (6)	S ₂ (7)
E–S0	-0.12	0.40	-0.14	0.48
...	0.02	0.07	0.04	0.10
Sa–Sc	1.74	-1.96	-0.87	2.57	-2.28	6.50
...	0.28	0.73	0.15	0.38	0.42	1.09
Sd–Im	0.17	2.05	-0.49	1.63	-0.94	2.97
...	0.27	0.70	0.05	0.13	0.14	0.36
Pec/merger	0.51	1.43	-0.59	2.08	-0.52	1.87
...	0.36	0.94	0.17	0.44	0.21	0.55

NOTE. — Coefficients for the linear dependence of the CAS parameters on the logarithm of the wavelength in nm. The second line for each type-bin lists the uncertainties on these coefficients. The coefficients are given for the linear-least-squares fit to the data within each type bin, resulting in the equation: $X = X_1 \times \log(\lambda_c) + X_2$, where X is the concentration index (C) for columns 2–3, the asymmetry index (A), for columns 4–5, and the clumpiness index (S) for columns 6–7. Note that better polynomial fits for C (E–S0), and for A and S (Sa–Sc) are given by Eq’s 6–8 in the text.

clumpiness index also decreases significantly with wavelength for all galaxy types. The reader should be advised that the linear fits of the wavelength dependence of A and S for Sa–Sc galaxies do not fit the data as well as the 2nd order polynomial fits presented in Eq’s 7–8.

Because the same galaxies were not observed at all wavelengths, it is more meaningful to determine the dependence of the CAS parameters on wavelength by examining the differences seen within individual galaxies, rather than fitting trends to the entire data set. Therefore, we also calculated the difference between the CAS parameters in R and U for each individual galaxy that met our reliability criteria, and which have CAS values

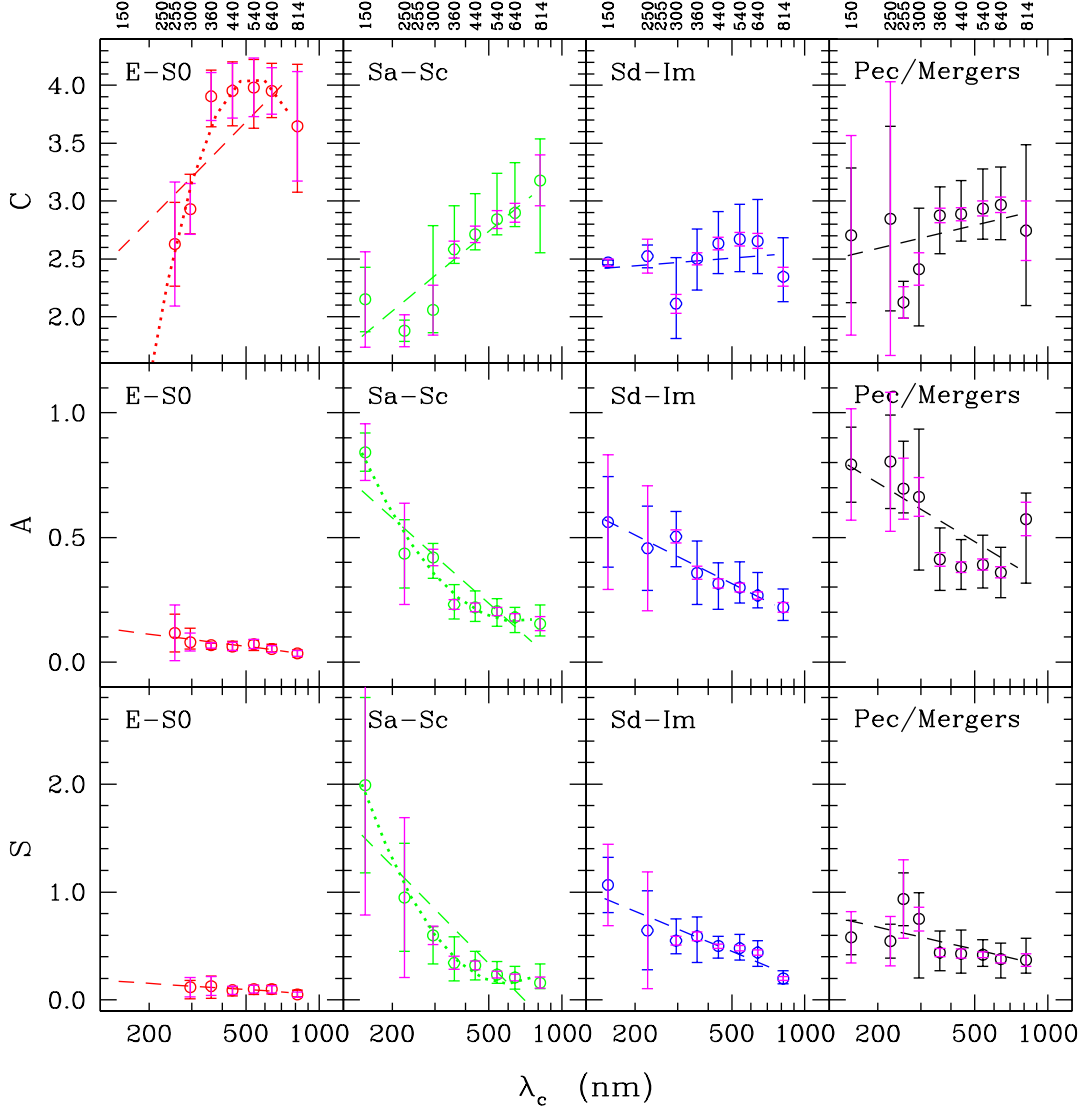


FIG. 17.— The median CAS parameters as a function of the central wavelength in nm (λ_c) of each filter. The values for different type-bins are separated into different panels, from left to right. Error bars with the same color as the data points show the 25–75% quartile ranges. Magenta error bars show the error on the median. Data that did not meet our reliability criteria, and CAS values < -0.2 are not included in the medians. Parameters for type-bins and filters with fewer than 2 galaxies are not plotted. Dashed lines are the linear-least-squares fit to the median CAS parameters. Dotted lines are the 2nd order polynomial fits to the data, shown only in the C panel for E–S0 galaxies, and the A and S panel for Sa–Sc galaxies. These may be the only panels where the trend is of higher order than linear. These fits show an increase in C, and a decrease in A and S with increasing rest-frame wavelength, although early-type galaxies (E–S0) are relatively constant in C, A, and S with increasing rest-frame wavelength longward of the Balmer break. Shortward of the Balmer break, the trend for early-type galaxies is more uncertain due to the low S/N of these intrinsically red galaxies in the UV images.

> -0.2 . We use these filters because we have higher number statistics in the ground-based VATT data, and all of the 143 VATT galaxies were consistently observed in U and R , but not necessarily in the HST and GALEX filter sets. We find median differences between C in the R - and U -band ($C_R - C_U$) of 0.081, 0.378, 0.139, and 0.135, for E–S0, Sa–Sc, Sd–Im, and peculiar/merging galaxies, respectively. A positive number indicates an increase in the index at longer wavelengths. This difference in C is significant within the scatter for individual galaxies (defined as half of the 25–75% quartile range of $C_R - C_U$) for E–S0 and Sa–Sc galaxies, which have a scatter of ± 0.048 and 0.121, respectively. This is less

significant for later-type galaxies, however as there is a larger range of possible $C_R - C_U$ values for individual galaxies (with a scatter of ± 0.162 for Sd–Im, and 0.152 for peculiar/mergers). The asymmetry index only varies significantly within the spread for E–S0 galaxies, with a small decrease in A from U to R ($A_R - A_U = -0.011$), and a scatter in $A_R - A_U$ of ± 0.008 . The difference between A in R and U is larger for the later-type galaxies, but so is the spread in values between individual galaxies. $A_R - A_U \pm$ the scatter in $A_R - A_U$ for Sa–Sc, Sd–Im, and mergers, respectively is: -0.057 ± 0.059 , -0.064 ± 0.078 , and -0.044 ± 0.071 . The clumpiness parameter also decreases at longer wavelengths, although the scatter is

large. $S_R - S_U \pm$ the scatter in $S_R - S_U$ for E-S0, Sa-Sc, Sd-Im, and mergers, respectively is: -0.030 ± 0.032 , -0.160 ± 0.130 , -0.140 ± 0.195 , and -0.065 ± 0.160 . So, even though there is a general increase in C and decrease in A and S toward longer wavelengths, the degree to which this difference occurs varies significantly between individual galaxies. The values presented here may be used as a correction to the general statistics of a large sample of galaxies, but cannot be applied with a large degree of certainty to any one individual galaxy.

7. CONCLUSIONS

Concentration, asymmetry, and clumpiness (CAS) indices are basic structural parameters of galaxies. Because the CAS parameters are based on the light distributions of galaxies, they describe quantifiable aspects of their morphologies. A difference in these parameters as a function of wavelength therefore contains information about how a galaxy's appearance changes with rest-frame wavelength, and leads to a measure of the morphological k-correction. This is important for high redshift studies, because at high redshift these galaxies are observed in their rest-frame UV. To quantify this, we have presented CAS parameter measurements for our sample of 199 mostly late-type and merging/peculiar galaxies observed in various combinations of filters spanning the far-UV through the near-IR.

Our results confirm those of previous studies, but over a much wider wavelength range that includes the UV: galaxies are more concentrated, less asymmetric, and less clumpy with redder color and earlier galaxy type. We find that normal and merging/peculiar galaxy type classes occupy different locations within the CAS parameter space, such that correlations between the CAS parameters can be used for statistical galaxy classification, but in a limited sense due to both intrinsic and observational scatter.

A general evolutionary trend as a merger progresses through its different stages can be drawn from these correlations, with mergers becoming significantly less concentrated, more asymmetric, and more clumpy than pre-mergers, then progressing back toward the normal galaxy parameter space, where they become merger remnants, which are more concentrated and slightly more asymmetric and clumpy than pre-mergers.

We find no significant difference in the CAS parameters for early-type galaxies (E-S0) at rest-frame wavelengths longward of the Balmer break. We cannot measure the wavelength dependence of the CAS parameters of early-type galaxies shortward of the Balmer break with great confidence, because these red galaxies have very low S/N in the GALEX and HST F255W and F300W filters, and because of the lack of good statistics in the far and mid-UV. However, we find that later type galaxies (S-Im and peculiar/mergers) observed at shorter wavelengths appear to be less concentrated, more asymmetric, and more clumpy than they would appear to be at longer wavelengths. Therefore, there is little to no morphological k-correction for the CAS parameters of early-type galaxies (E-S0) in the optical, but a more significant correction for all other later galaxy types at all wavelengths between the far-UV and near-IR.

These nearby-galaxy results can be used as a benchmark for interpreting the CAS morphological parameters

of high redshift galaxies observed in the rest-frame UV. The morphological k-correction derived here will help us to determine how much of the difference we see in the morphologies of high redshift galaxies is purely due to band-pass shifting effects, and a comparison of the structural CAS parameters between low and high redshift galaxies will provide some understanding of galaxy evolution. We will address these aspects of the high redshift Universe in a future paper (Conselice, et al. 2007, in preparation).

The current study shows that one cardinal improvement to this work would be to obtain a much larger sample in the mid-UV at $\sim 100\times$ the sensitivity, which WFC3 will be able to do after SM4 is launched. Such studies will be critical to help interpret the 10's of millions of distant galaxy images JWST will observe after 2013 in the rest-frame UV, at $\lambda \gtrsim 1\mu\text{m}$ and $z \gtrsim 2$.

Based on observations with the VATT: the Alice P. Lennon Telescope and the Thomas J. Bannan Astrophysics Facility. This research was partially funded by NASA grants GO-8645.01-A, GO-9124.01-A and GO-9824.01-A, awarded by STScI, which is operated by AURA for NASA under contract NAS 5-26555. Additional funding was provided by GALEX grant #GALEXGI04-0000-0036, and the NASA Space Grant Graduate Fellowship at ASU. We wish to thank the entire staff of Steward Observatory and the Vatican Advanced Technology Telescope for all of their help and support on this project. We especially thank Drs. Richard Boyle, Matt Nelson, and Chris Corbally for offering so much of their time and expertise during our VATT observing runs. CJC thanks the National Science Foundation for support through an Astronomy and Astrophysics Fellowship and PPARC for support at the University of Nottingham. This research has made use of the NASA/IPAC Extragalactic Database (NED) which is operated by the Jet Propulsion Laboratory, California Institute of Technology, under contract with the National Aeronautics and Space Administration. This research has also made use of NASA's Astrophysics Data System.

REFERENCES

- Abraham, R. G., Valdes, F., Yee, H. K. C., van den Bergh, S. 1994, *ApJ*, 432, 75
- Abraham, R. G., Tanvir, N. R., Santiago, B. X., Ellis, R. S., Glazebrook, K., & van den Bergh, S. 1996, *MNRAS*, 279, L47
- Baugh, C. M., Cole, S., Frenk, C. S., & Lacey, C. G. 1998, *ApJ*, 498, 504
- Bershady, M. A., Jangren, A., & Conselice, C. J. 2000, *ApJ*, 119, 2645
- Bertin, E., and Arnouts, S. 1996, *AJ*, 117, 393
- Bohlin, R. C., et al. 1991, *ApJ*, 368, 12
- Cohen, S. H., Windhorst, R. A., Odewahn, S. C., Chiarenza, C. A., & Driver, S. P. 2003, *AJ*, 125, 1762
- Cohen, S. H., et al. 2006, *ApJ*, 639, 731
- Cole, S., Aragon-Salamanca, A., Frenk, C. S., Navarro, J. F., & Zepf, S. E. 1994, *MNRAS*, 271, 781
- Conselice, C. J. 1997, *PASP*, 109, 1251
- Conselice, C. J., Bershady, M. A., & Jangren, A. 2000, *ApJ*, 529, 886
- Conselice, C. J., Bershady, M. A., Dickinson, M., & Papovich, C. 2003, *AJ*, 126, 1183
- Conselice, C. J. 2003, *ApJS*, 147, 1
- Conselice, C. J., et al. 2004, *ApJ*, 600, 139L
- Conselice, C. J., Blackburne, J. A., & Papovich, C. 2005, *ApJ*, 620, 564
- Conselice, C. J. 2006, *ApJ*, 638, 686
- Corbin, M. R., Urban, A., Stobie, E., Thompson, R. I., & Schneider, G. 2001, *ApJ*, 551, 23
- de Vaucouleurs, G., de Vaucouleurs, A., Corwin, H. G., Buta, R. J., Paturel, G., & Fouque, P. 1991, *Third Reference Catalogue of Bright Galaxies* (Springer, New York)
- Driver, S. P., Windhorst, R. A., Ostrander, E. J., Keel, W. C., Griffiths, R. E., & Ratnatunga, K. U. 1995, *ApJ*, 449, L23
- Driver, S. P., Fernandez-Soto, A., Couch, W. J., Odewahn, S. C., Windhorst, R. A., Phillips, S., Lanzetta, K., & Yahil, A. 1998, *ApJ* 496, L93
- Ellis, R. S. 1997 *ARA&A*, 35, 389
- Giavalisco, M., et al. 2004, *ApJ*, 600, 93
- Glazebrook, K., Ellis, R., Santiago, B., & Griffiths, R. 1995, *MNRAS*, 275, L19
- Heckman, T. M., et al. 2005, 619, 35
- Hibbard, J. E., van Gorkom, J. H., Rupen, M. P., & Schiminovich, D. 2001, *ASPC*, 240, 657
- Hill, J. K., et al. 1992, *ApJ*, 395, L37
- Im, M., Griffiths, R. E., Naim, A., Ratnatunga, K. U., Roche, N., Green, R. F., & Sarajedini, V. 1999, *ApJ*, 510, 82
- Isserstedt, J. & Schindler, R. 1986, *A&A*, 167, 11
- Jansen, R. A. 2000, Ph.D. Thesis, University of Groningen
- Kauffmann, G., Nusser, A., & Steinmetz, M. 1997, *MNRAS*, 286, 795
- Kuchinski, L. E., et al. 2000, *ApJS*, 131, 441
- Kuchinski L. E., Madore, B. F., Freedman, W. L., & Trewhella, M. 2001, *AJ* 122, 729
- Lotz, J. M., Primack, J., & Madau, P. 2004, *AJ*, 128, 163
- Marcum, P. M., et al. 2001, *ApJS*, 132, 129
- Martin, D. C., et al. 2005, *ApJL*, 619, 1
- Nagashima, M., Totani, T., Gouda, N., & Yoshii, Y. 2001, *ApJ*, 557, 505
- Nagashima, M., Yoshii, Y., Totani, T., & Gouda, N. 2002, *ApJ*, 578, 675
- Odewahn, S. C., Windhorst, R. A., Driver, S. P., & Keel, W. C. 1996, *ApJ*, 472, L13
- Papovich, C., Dickinson, M., Giavalisco, M., Conselice, C. J., & Ferguson, H. C. 2005, *ApJ*, 631, 101
- Petrosian, V., *ApJL*, 209, 1
- Roukema, B. F., Quinn, P. J., Peterson, B. A., & Rocca-Volmerange, B. 1997, *MNRAS*, 292, 835
- Schade, D., Lilly, S. J., Crampton, D., Hammer, F., Le Fevre, O., & Tresse, L. 1995, *ApJL*, 451, 1
- Takamiya, M. 1999, *ApJS*, 122, 109
- Taylor, V. A., Jansen, R. A., & Windhorst, R. A. 2004, *PASP*, 116, 762
- Taylor, V. A., Jansen, R. A., Windhorst, R. A., Odewahn, S. C., & Hibbard, J. E. 2005, *ApJ*, 630, 784
- van den Bergh, S., Cohen, J. G., Hogg, D. W., & Blandford, R. 2000, *AJ*, 120, 2190
- van Dokkum, P. G., Franx, M., Fabricant, D., Kelson, D. D., & Illingworth, G. D. 1999, *ApJ*, 520, L95
- White, S. D. M. 1979, *MNRAS*, 189, 831
- White, S. D., & Frenk, C. S. 1991, *ApJ*, 379, 52
- Windhorst, R. A., et al. 2002, *ApJS*, 143, 113